Title

Control and control-oriented modeling of PEM water electrolyzers: A review

Journal

International Journal of Hydrogen Energy, 48(79)

ISSN

0360-3199

Authors

Majumdar, Abhigyan
Haas, Meridian
Elliot, Isabella
et al.

Publication Date

2023-09-01

DOI

10.1016/j.ijhydene.2023.04.204

Control and Control-Oriented Modeling of PEM Water Electrolyzers: A Review

Abhigyan Majumdar[a,1], Meridian Haas[a,1], Isabella Elliot[a], Shima Nazari[a]

[a]*Department of Mechanical and Aerospace Engineering, University of California, Davis, CA, 95616, USA*

Abstract

As the most abundant element in the universe, hydrogen is a promising energy carrier for decarbonizing various economic sectors. Green hydrogen production from water electrolysis is critical to the success of this path with polymer electrolyte membrane (PEM) water electrolyzer (WE) as a key technology due to its quick dynamic response and high energy efficiency. Nevertheless, vigorous control algorithms are necessary to maximize the performance, efficiency, and usable lifetime of PEM WEs. This review attempts to collate the modeling frameworks relevant to controller design and provides a survey of various control techniques used in literature to overcome the challenges associated with the transient operation of PEM WEs. To better understand the underlying physics and the coupling between different subsystems, we first review control-oriented electrochemical, thermal, mass transport, and equivalent circuit models. We identify manipulable system variables and control knobs that can be employed for a better system operation in the next step, and finally, we discuss different controllers used in literature, including traditional control approaches, optimal control methods, and other advanced techniques such as nonlinear and neural network controllers.

Keywords: Hydrogen, PEM Water Electrolyzer, Modeling, Control

Highlights

- Review of control-oriented models of proton exchange membrane water electrolyzers
- Description of electrolyzer degradation and efficiency modeling
- Survey of available control actuators and control techniques in literature
- Discussion of the open challenges in modeling and control development

1. Introduction

In the face of climate change, hydrogen is envisioned as an energy carrier for heavy transportation applications and difficult to electrify industries and processes [1, 2, 3]. While the applications of hydrogen are numerous, the successful transition to a hydrogen economy depends on the efficiency and sustainability of the hydrogen production process. Most of the present hydrogen production in the world is that of gray hydrogen, meaning that it is produced from fossil fuels like natural gas through methods such as steam reforming [4, 5].

Green hydrogen is produced from renewable energy sources using water electrolysis. In this regard, low temperature water electrolysis technologies like Proton Exchange Membrane or Polymer Electrolyte Membrane (PEM) Water Electrolyzers (WE) are particularly interesting due to their technical maturity, high efficiency, and quick dynamic response. The green hydrogen produced from PEM WEs can be consumed in various economic sectors including power, transportation, and industrial systems, which respectively account for 25%, 27%, and 24% of greenhouse gas emissions in the US [6]. In particular, hydrogen based decarbonization of sectors like iron and steel production[7], shipping [8], heavy-duty land transportation [9], and aviation [10] have received great interest in recent years. Efforts have also been made to adapt combustion engines from internal combustion engines [11] to heavy-duty gas turbines [12] to run on hydrogen fuel.

Among the various applications, the coupling of PEM WEs with intermittent renewable energy sources (RES) like wind [13] and solar [14, 15, 16] have gained extra attention in recent years. PEM WE can serve as a dynamic on-demand load for such systems to maximize capacity utilization and increase grid resiliency, while also providing green hydrogen for later power production. Nevertheless, the generation from PV panels is highly sensitive to variations in solar irradiance, cloud cover, incidence angle, and temperature, which results in a highly transient power profile. The same is true for wind turbines, where the generated power depends on the constantly changing wind speed [13]. It has been shown that direct coupling of PEM WEs to such highly transient sources is detrimental to both the stack life and efficiency. For instance, Clarke et al. [14] noted a reduction in stack efficiency from 91% to 65% in 4 months of direct coupled operation. In another work, Kosonen et al. [17] showed electrolyzers connected directly to PV systems need some input power filtering through energy buffers such as a battery storage.

The above findings highlight the critical role of control system design in the longevity and performance optimization of

[1]Equal contribution authors

PEM WEs [18, 19]. Controller development relies on relatively simple plant models that can predict the system behavior with sufficient accuracy. Over the past decade, there has been an extensive effort in modeling of PEM WEs. Yodwong et al. provide a survey on simple equivalent circuit models (ECM) [20]. Electrochemical models are reviewed in various studies by Hernández-Gómez et al. [21], Abdol Rahim et al. [22], Falcao et al. [23], and Olivier et al. [24]. The mass transport [22, 23, 24] and thermal models [23, 24] are also surveyed in different studies. Järvinen et al. [25] provides a MATLAB toolbox based on a review of electrochemical models. Reviews on more complex models such as fluid dynamic models [24] and Computational Fluid Dynamics (CFD) based on Electrochemical Impedance Spectroscopy (EIS) [26] are also provided in the literature. Moreover, several review papers address the control design of PEM hydrogen fuel cells [27, 28, 29], however to the best of the authors' knowledge such a survey is nonexistent for PEM WEs. Therefore, this review focuses for the first time specifically on the control system development and control-oriented modeling of PEM WEs.

Control-oriented models are generally characterized as algebraic or Ordinary Differential Equations (ODEs) used to predict system dynamics during transient operation. However, we include few multi-physics models based on Partial Differential Equations (PDEs) for the sake of comprehensivity and because they were used in control system design or analysis. The remainder of this paper is organized as follows. In the first part, we introduce the principles of water electrolysis in a PEM WE. Next, we discuss and classify models relevant to control design including electrochemical models, thermal models, mass transport models, equivalent circuit models, and degradation and efficiency models. In the next part, we introduce the operational deployment of PEM WEs and control challenges faced in their transient operation. Then we present the different control knobs and manipulable system variables that can be employed for improved performance and various control methods observed in the literature are introduced next. We conclude the paper by identifying the research gaps and possible directions for future work.

2. Water Electrolysis

The Structure of PEM Electrolyzers consists of a stack of multiple unit cells, each having an anode and a cathode section, separated by the polymer electrolyte membrane, and sandwiched between current distributing plates. A schematic diagram of a PEM WE is shown in Fig. 1. The membrane and the electrodes are together called the Membrane Electrode Assembly (MEA). The membrane is usually made of Nafion or its derivatives, and works as a separator that keeps the anodic and cathodic products from mixing. The anode and cathode are each split into flow channels, Porous Transport Layer (PTL), and active material, as shown in Fig. 1. The anodic flow channels are designed to ensure feed water reaches the entire active area of the electrode with uniform pressure. The cathodic flow channels on the other hand are designed to effectively evacuate hydrogen gas [30]. The PTL also aids the flow channels in this purpose and distributes the reactants equally. In the anode active region, noble-metal based catalysts are coated on carbon micro-particles to facilitate the Oxygen Evolution Reaction (OER) or the anode half-reaction, under the influence of an induced electric potential

$$2H_2O \rightarrow 4H^+ + O_2(g) + 4e^-. \quad (1)$$

The protons flow through the PEM membrane, aided by the sulfonic acid groups on Nafion, while the electrons flow through the external circuit to the cathode [31]. Hence, the membrane also works as an electrolyte. The oxygen gas ventilates through the anodic flow channels, mixed with water vapour and traces of hydrogen that crossover through the membrane. In the cathode, the electrons from the external circuit combine with the protons from the anode and produce hydrogen gas. This is called the cathode half-reaction, or the Hydrogen Evolution Reaction (HER)

$$4H^+ + 4e^- \rightarrow 2H_2(g). \quad (2)$$

Thus, the overall balanced chemical reaction in the cell is

$$2H_2O(l) \rightarrow 2H_2(g) + O_2(g). \quad (3)$$

The hydrogen created at the cathode side mixes with crossed over water vapor. For long term storage or usage, this gas needs to be dehumidified and pressurized/liquefied using gas dryers, mechanical compressors, intercoolers, and cryochillers. Along with upstream components like water filtration system, pumps, and heat exchangers, they are together called the Balance of Plant components (BOP).

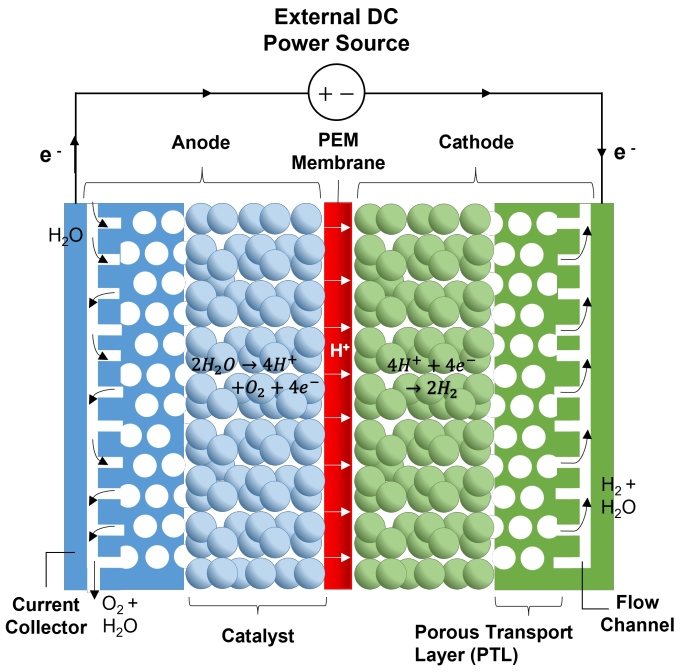

Figure 1: Schematic Diagram of PEM Water Electrolyzer Including the Flow of Species and the Half-Reactions.

The structure and principle of operation of PEM WEs are similar to that of PEM Fuel Cells (FC) in which the opposite reaction occurs to produce electric potential and water by oxidizing hydrogen. Unlike PEM WEs, there is rich literature on PEM FCs [32, 33, 34], and thus PEM FC models played an important role in developing models of PEM WEs [21]. In the next section, we present electrolyzer modeling techniques of varying fidelity that provide a deeper insight into the operation of these devices and and their various components.

3. Modeling

Design of a PEM WE controller requires an accurate model to describe the dynamic operation. A control-oriented model is characterized by a simple set of equations that represent the dynamics of the system.

The physical domains within an electrolyzer are interconnected such that changes to one impacts another. Therefore, physics-based water electrolyzer models require the coupling of different submodels to emulate this behavior. Models use a combination of electrochemical, thermal, and mass transport submodels to fully describe operation of the stack. Figure 2 shows the modeling domains and their connections to processes inside of the electrolyzer cell.

- *Electrochemical models* describe the electrical potential required for the electrolysis reaction and the overpotential caused by irreversible processes. Such models quantify the voltage drop due to inefficiencies within the cell, reflecting their impact on cell operation.
- *Thermal models* capture the heat transfer and temperature dynamics in the system. They also model the irreversibilities that contribute to heat generation.
- *Mass transfer* and *reaction models* simulate the movement of water, oxygen, and hydrogen across the cell. Bubble formation and proton transfer across the membrane are also included in these models.

In this section, each submodeling technique is described and the models found in literature are categorized.

Then, the simpler models that quantify the voltage of an electrolyzer with an equivalent electrical circuit are discussed. These models emulate the electrical dynamics with empirically derived resistor and capacitor elements. Finally, discussions of membrane degradation models and the attempts to quantify the efficiency of PEM WEs are included.

3.1. Electrochemical Models

The electric potential applied to the electrodes to induce a reaction drives the operation of a water electrolyzer. Thus, modeling the building blocks of such voltage enables a deep understanding of the system efficiency and is imperative to control design. This section will develop the different electrochemical models with increasing complexity. Table 1 classifies the literature by the electrochemical model included in each. The electrochemical models introduced in this section can predict and simulate various parameters in a cell.

The electrolyzer cell voltage, V_{cell}, is separated into the following building blocks which describe different losses and irreversibilities in a water electrolyzer

$$V_{cell} = V_{rev} + V_{ohm} + V_{act} + V_{con} + V_{bub} \tag{4}$$

where,

- Reversible potential, V_{rev}, describes the required theoretical voltage, from thermodynamics, for the electrolysis reaction.
- Ohmic overpotential, V_{ohm}, models the resistance of the membrane.
- Activation overpotential, V_{act}, describes the potential needed to initiate the reaction at the electrodes.
- Concentration overpotential, V_{con}, captures the voltage loss due to mass transfer limitations and the concentration gradients in the anode and cathode.
- Bubble overpotential, V_{bub}, models the irreversibilities from bubble formation on the electrodes and membrane.

Such models are categorized in Table 1.

3.1.1. Reversible Potential

In the simplest case, the reversible voltage is assumed to be a constant

$$V_{rev} = V_0 \tag{R1}$$

where V_0 models the reversible voltage at standard operating conditions [39]. However, more complex models include another term to capture the variation of reversible voltage for different operating conditions. The Nernst equation quantifies the variation of V_{rev} with respect to temperature and pressure [51]

$$V_{rev} = V_0 + \frac{RT}{2F} ln\Big(\frac{P_{H_2} P_{O_2}^{1/2}}{P_{H_2O}}\Big) \tag{R2}$$

where T is the temperature, R is the universal gas constant, and F is Faraday's constant. The partial pressures of hydrogen, oxygen, and water are denoted with P_{H_2}, P_{O_2}, and P_{H_2O}, respectively. The exponents are based on their stoichiometric coefficients in the full electrolysis reaction in Eq. (3).

Standard reversible potential is computed from the change in Gibbs free energy, ΔG, which is the energy needed to split water into gaseous oxygen and hydrogen [40]

$$V_0 = \frac{\Delta G}{zF} \tag{V1}$$

where z is the stoichiometric coefficient used to represent the number of electrons exchanged during the reaction, which is 2 for each molecule of hydrogen gas. Other models use empirical expressions that rely on temperature only. In increasing order

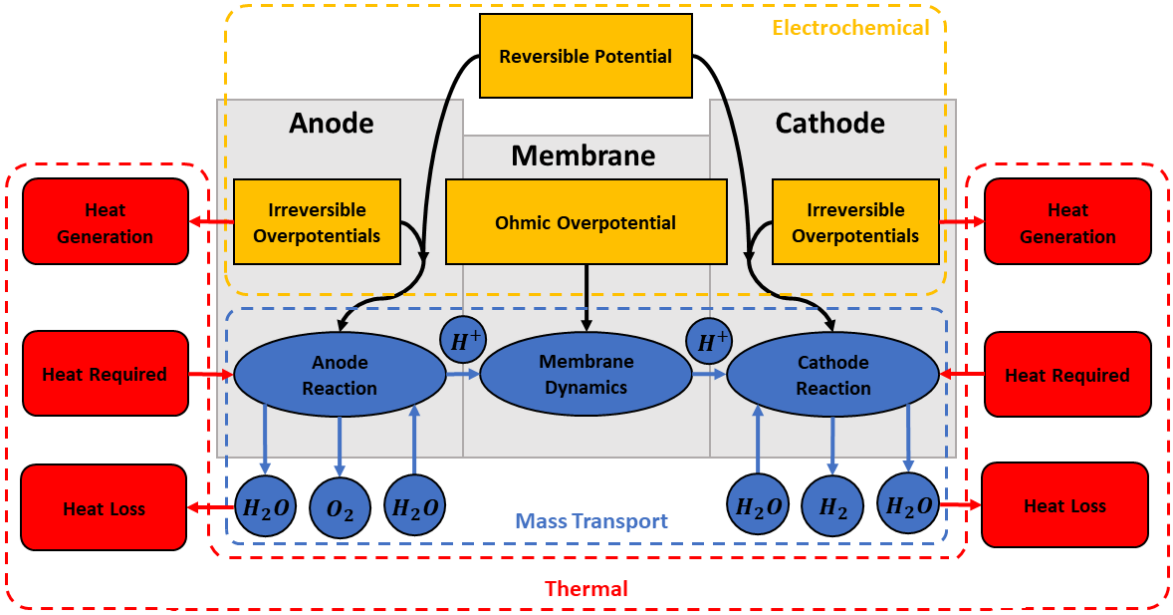

Figure 2: Coupling of the Electrochemical, Thermal, and Mass Transport Submodels for PEM Water Electrolyzers.

of complexity, the following temperature based correlations are used in literature to describe the standard reversible potential

$$V_0 = 1.229 - 8.5 \cdot 10^{-4}(T - 298) \tag{V2}$$

$$V_0 = 1.5241 - 1.2261 \cdot 10^{-3}T + 1.1858 \cdot 10^{-5}T\ln(T) + 5.6692 \cdot 10^{-7}T^2 \tag{V3}$$

$$V_0 = 1.5184 - 1.5421 \cdot 10^{-3}T + 9.523 \cdot 10^{-5}T\ln(T) + 9.84 \cdot 10^{-8}T^2 \, . \tag{V4}$$

Table 1 includes a categorization of the papers that use each one of these relationships.

3.1.2. Ohmic Overpotential

The ohmic overpotential models the irreversibility which arises from the finite conductivity of the cell. Ohm's Law defines the relationship of the current and voltage of the electrolyzer with the equivalent resistance

$$V_{ohm} = i_{el}R_{eq} \, . \tag{5}$$

The value of R_{eq} can include the electric resistance of different elements in the cell, however, it is common to include the resistance of the membrane only, as it possesses the smallest conductivity

$$R_{eq} = R_{mem} \, . \tag{O1}$$

Note that this loss describes the resistance to protons crossing the membrane and it depends on the pressure, temperature and water content of the membrane among other factors. The membrane resistance can be computed as

$$R_{mem} = \frac{\delta_{mem}}{\sigma_{mem}} \tag{6}$$

where δ_{mem} is the thickness of the membrane and σ_{mem} represents the conductivity of the membrane described by

$$\sigma_{mem} = (0.005139\lambda - 0.00326)exp\Big[1268\Big(\frac{1}{303} - \frac{1}{T}\Big)\Big] \tag{7}$$

where λ is the humidification of the membrane [64] and describes the concentration of water in the membrane.

Some models account for the resistances in the electrodes, R_{elec} as well, such that the equivalent resistance is described as

$$R_{eq} = R_{mem} + R_{elec} \, . \tag{O2}$$

3.1.3. Activation Overpotential

The activation overpotential, V_{act}, represents the voltage drop due to initiating the transfer of protons. It directly represents the speed of the reactions and is composed of $V_{act,a}$, the activation overpotential for the anode, and $V_{act,c}$, the activation overpotential for the cathode, such that

$$V_{act} = V_{act,a} + V_{act,c} \, . \tag{8}$$

Different expressions are proposed in literature to determine the activation overpotential required for both the anode and cathode. Based on the Butler-Volmer equation, simplified for oxidation at the anode and reduction at the cathode, the following variations of the activation overpotential are suggested

$$V_{act,k} = \frac{RT}{\alpha_k zF} ln\Big(\frac{i_k}{i_{k0}}\Big) \quad \text{for } k = a, c \tag{A1}$$

Author	Reversible	Standard Reversible	Ohmic	Activation	Concentration	Bubble	Reference
Abdin et al.	R2	V2	O2	A2	C1	—	[35]
Abomazid et al.	R2	V1	O1	A3	C2	—	[36]
Afshari et al.	R2	V2	O2	A1	C1	—	[37]
Agbli et al.	R2	V4	O1	A3	C1	B3	[38]
Ahmadi et al.	R1	V2	O1	A3	—	—	[39]
Aubras et al.	R2	V1	O1	A2	—	—	[40]
Awashti et al.	R2	V2	O1	A2	—	—	[41]
Biaku et al.	R2	V2	O1	A3	—	—	[42]
Chandesris et al.	R2	V1	O2	A1	—	—	[43]
Choi et al.	R2	V2	O1	A3	—	—	[44]
da Costa Lopes et al.	R1	V1	O1	A3	—	—	[45]
Dale et al.	R2	V3	O1	A3	—	—	[46]
Espinosa-López et al.	R2	V2	O2	A3	negligible	—	[47]
Fragiacomo et al.	R1	not defined	O1	A1	C2	—	[48]
Gabrielli et al.	R2	V1	O2	A2	C1	—	[49]
Garcia-Valverde et al.	R1	V4	O2	A1	—	B3	[50]
Görgün et al.	R2	V1	O1	A1	—	—	[51]
Grigoriev et al.	R2	V2	O1	A1	—	—	[52]
Han et al.	R2	V2	O2	A2	C1	—	[53]
Keller et al.	R2	V1	O2	A1	negligible	—	[54]
Kim et al.	R2	V1	O2	A2	C1	—	[55]
Koundi et al.	R2	V3	O1	A2	negligible	—	[56]
Lebbal et al.	R2	V1	O1	A1	C2	—	[57]
Lee et al.	R2	not defined	O1	A1	—	—	[58]
Liso et al.	R2	V1	O1	A2	C1	—	[59]
Laoun et al.	R2	V1	O1	A2	C1	—	[15]
Marangio et al.	R2	V1	O2	A2	C1	—	[60]
Mohamed et al.	R2	V1	O2	A1	C2	—	[61]
Moradi Nafchi et al.	R2	V2	O2	A2	C1	—	[62]
Ni et al.	R1	not defined	O1	A2	—	—	[63]
Ogumerem et al.	R2	V2	O1	A2	—	B2	[64]
Ojong et al.	R2	V1	O2	A2	C1	B1	[65]
Olivier et al.	R2	V4	O2	A3	—	—	[66]
Rahim et al.	R1	V1	O2	A1	negligible	—	[67]
Ruuskanen et al.	R2	V2	O1	A2	negligible	—	[68]
Sarrias-Mena et al.	R2	V2	O1/O3	A2/A3	C1	—	[69]
Sartory et al.	R2	V1	O2	A2	C2	—	[70]
Sawada et al.	R1	V1	O2	A3	—	—	[71]
Schalenbach et al.	R2	V1	O1	—	—	—	[72]
Scheepers et al.	R2	V2	O2	A3	—	—	[73, 74]
Schnuelle et al.	R2	V1	O2	A3	—	—	[75]
Sood et al.	R2	V4	O2	A3	—	—	[76]
Tabanjat et al.	R2	V4	O1	A3	C1	—	[77]
Tijani et al.	R1	V1	O2	A2,A3	C1	—	[78, 79]
Tjarks et al.	R2	V1	O1	not defined	negligible	—	[80]
Toghyani et al.	R2	V2	O2	A3	C1	—	[81]
Yigit et al.	R2	V1	O1	A2	—	—	[82]
Zhang et al.	R2	V2	O1	A3	C3	—	[83]
Zhao et al.	R2	not defined	O1	A3	—	—	[84, 85]

Table 1: Electrochemical Models in Literature.

$$V_{act,k} = \frac{RT}{\alpha_k F} sinh^{-1}\Big(\frac{i_k}{2i_{k0}}\Big) \quad \text{for } k = a, c \tag{A2}$$

$$V_{act,k} = \frac{RT}{\alpha_k z F} sinh^{-1}\Big(\frac{i_k}{2i_{k0}}\Big) \quad \text{for } k = a, c \tag{A3}$$

where α_a and α_c are the charge transfer coefficients for the anode and cathode. Since some models approximate these coefficients to be symmetrically equal to 0.5, and the stoichiometric coefficient, z, has a value of 2, the product of these variables is 1. Thus, such models simplify the expression by omitting both variables [44]. i_a and i_c are the current densities of the anode and cathode, and i_{a0} and i_{c0} are the respective exchange current densities.

3.1.4. Concentration Overpotential

The concentration overpotential, also denoted as the diffusion overpotential, models the resistance due to the mass transfer within the cell. At low current densities, the ohmic and activation overpotentials are significantly larger than the concentration overpotential, thus the concentration overpotential is often neglected in these operating conditions. Concentration overpotential can be described as the sum of the concentration overpotentials in the anode and cathode, $V_{con,a}$ and $V_{con,c}$, respectively

$$V_{con} = V_{con,a} + V_{con,c} \ . \tag{9}$$

The Nernst equation, in some literature, is used to compute $V_{con,a}$ and $V_{con,c}$

$$V_{con,a} = \frac{RT}{z_a F} ln\Big(\frac{C^{\text{mem}}_{O_2}}{C^{\text{mem}}_{O_2,0}}\Big) \tag{C1}$$

$$V_{con,c} = \frac{RT}{z_c F} ln\Big(\frac{C^{\text{mem}}_{H_2}}{C^{\text{mem}}_{H_2,0}}\Big) \tag{C1}$$

where $C^{\text{mem}}_{O_2}$ is the concentration of oxygen on the membrane-anode interface, and $C^{\text{mem}}_{H_2}$ is the concentration of hydrogen on the membrane-cathode interface [35]. The values of z_a and z_c, the stoichiometric coefficients, are different for the anode and cathode sub-reactions. Specifically, on the anode side z_a is 4 based on Eq. (1) and for the cathode z_c is 2 from Eq. (2).

Another model employed in literature to compute the concentration overpotential is

$$V_{con} = \frac{RT}{\beta z F} ln\Big(1 + \frac{i_{el}}{i_{lim}}\Big) \tag{C2}$$

where β is an empirically derived coefficient and i_{lim} is the limiting current density based on the diffusion capabilities. These values are determined from curve fitting of experimental data [57].

The model introduced by Zhang et al. [83] instead describes the concentration irreversibilities with the limiting current density, i_{lim}, in the following equation

$$V_{con} = i_{el}\Big(\beta_1 \frac{i_{el}}{i_{lim}}\Big)^{\beta_2} \tag{C3}$$

where β_1 is a function of temperature and pressure of oxygen and β_2 is a constant. Table 1 also categorizes different concentration overpotential models used in literature.

3.1.5. Bubble Overpotential

The hydrogen and oxygen that form in the water electrolysis reaction are gaseous and therefore can cover some active sites and reduce the active area of the electrode. Bubbles also influence the operation of the cell by decreasing the water input to the membrane or by creating hot spots that the circulating water does not cool. The main variable that describes bubbles is the bubble coverage, Θ, which is defined as

$$\Theta = \Theta_0\Big[1 + \frac{v^2(\frac{1}{\Theta_0} - 1)}{v_0^2(\frac{1}{\Theta_0} - 1) + 1}\Big]^{-2} \ . \tag{10}$$

Bubble coverage describes the sum of the pore to bubble ratio and the water starvation ratio on the anode side of the membrane. In this definition, Θ and Θ_0 are the bubble coverage fractions when water is flowing and stagnant, respectively, and v_0 and v are the free flow and forced flow velocities. Most literature doesn't fully address the influence of bubble formation. However, some models describe bubble effects with the Butler-Volmer equation modified to be non-linear based on experimental analysis of the bubble overpotential within the region of mass transport [65]

$$V_{bub} = \frac{RT}{\alpha_a z F}\Big(\frac{1}{1 - \Theta}\Big)^2 \ . \tag{B1}$$

Alternatively, bubble coverage can also be used to correct the current in the ohmic overpotential [64]. The corrected current density, i_c, replaces the electrolyzer current density in Eq. (5)

$$i_c = \frac{i_{el}}{1 - \Theta} \ . \tag{B2}$$

Bubble effects are included in the anodic concentration overpotential in other models [38]. Such descriptions replace the concentration irreversibilites in the anode in Eq. (C1) with the following term

$$V_{con,a} = \frac{RT}{\alpha_a z F} ln\Big(\frac{\frac{i_a}{i_{a0}}}{1 - \frac{i_a}{i_{lim,a}}}\Big) \tag{B3}$$

to include the inefficiencies that result from bubbles as modeled with $i_{lim,a}$, the limiting current density of the anode. Table 1 includes bubble overpotential descriptions in literature.

A polarization curve is developed in Fig. 3 from the full model developed by Ojong et al. [65]. This model includes the reversible voltage and each of the described irreversible overpotentials, namely (R2), (V1), (O2), (A2), (C1), and (B1).

The next section describes thermal models of PEM water electrolysis.

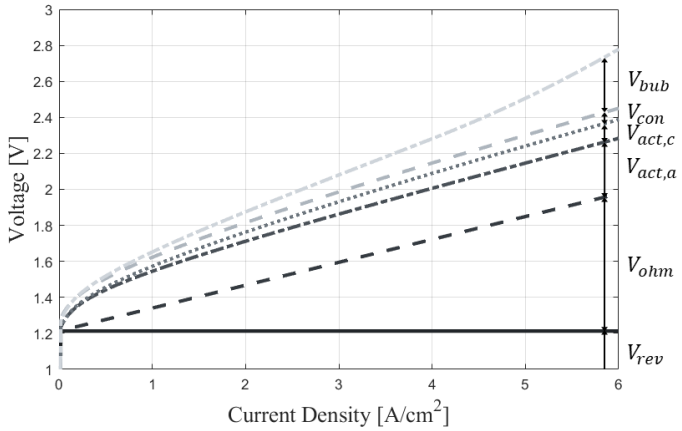

Figure 3: Example of Polarization Curve of a PEM Electrolyzer Recreated from the Model by Ojong et al. [65] The Cell Voltage is Separated into the Reversible Potential and Various Overpotentials.

3.2. Thermal Models

Temperature is a critical variable in operation of an electrolyzer cell, thus many models incorporate a thermal submodel to track temperature variation during cell operation. Temperature contributes to cell aging and degradation in addition to influencing the system efficiency and safety. The electrolysis reaction is endothermic, but the irreversible processes within a WE cell are exothermic thus, thermal models of PEM WEs can be complex. Such models can take the form of ordinary differential equations (ODE) that neglect temperature variation with position, or they can be in the form of more complicated partial differential equations (PDE) that capture spatial variations of temperature. As mentioned before, the focus of this review is the models described by ODEs since PDE thermal models are generally too computationally expensive for control methods. Table 2 summarizes the thermal models used in literature.

Within an ODE thermal model, the First Law of thermodynamics energy balance for an open system along with a lumped capacitance model is used to describe the temperature dynamics as a first order ODE

$$C_{th}\frac{dT}{dt} = \sum h_i^{in} N_i^{in} - \sum h_i^{out} N_i^{out} + \dot{Q}_{net} \tag{11}$$

where h_i is the specific enthalpy of species i, and N_i is the molar flow rate of the corresponding species in or out of the electrolyzer [64]. The lumped thermal capacitance or overall thermal capacity, C_{th}, is the sum of the component thermal capacities

$$C_{th} = \sum \rho_j V_j C_{p,j} \tag{12}$$

in which ρ_j, V_j, and $C_{p,j}$ are the values for density, volume, and heat capacity of each component, respectively [49]. The net heat generation, $\dot{Q}_{net}$, is composed of varied heat sources and sinks in the system

$$\dot{Q}_{net} = \dot{Q}_{gen} - \dot{Q}_{loss} - \dot{Q}_{cool} - \dot{Q}_{misc} \tag{13}$$

the terms described in the net heat generation of the system include $\dot{Q}_{gen}$, $\dot{Q}_{loss}$, $\dot{Q}_{cool}$, and $\dot{Q}_{misc}$ which describe heat generation, loss, cooling, and other miscellaneous phenomena, respectively.

The first of such terms, which describes the transient heat generation from the electrolysis process, can be expressed as

$$\dot{Q}_{gen} = N_c(V_{cell} - V_{th})I \tag{G1}$$

where I is the current, which is calculated as product of the current density, i_{el}, and the area of the cell, A. The variable N_c, the number of cells in the stack, allows the total heat generation of the electrolyzer to be calculated. The thermoneutral voltage, V_{th}, describes the heat energy contained in the chemical reaction

$$V_{th} = \frac{\Delta H}{2F} \tag{14}$$

where ΔH, the change in enthalpy from the electrolysis reaction is expressed by

$$\Delta H = \Delta G + T\Delta S \tag{15}$$

in which the temperature of the cell, T, is known and ΔG and ΔS describe the change in Gibbs free energy and entropy for the reaction, respectively [57].

The heat generation is also calculated using the sum of the overpotentials in other models, which are the largest form of heat generation

$$\dot{Q}_{gen} = \sum V_{over} I\ . \tag{G2}$$

The overpotential term includes the ohmic overpotential, activation overpotential, concentration overpotential, and bubble overpotential [83].

Various models are introduced in literature for the transient heat loss. Fragiacomo et al. [48] employ the following expression

$$\dot{Q}_{loss} = \frac{1}{R_{th}}(T - T_{amb}) \tag{L1}$$

in which T_{amb} is the ambient temperature, and R_{th} is the thermal resistance. The total heat that can be lost to the ambient surroundings is a function of the WE cell's temperature difference from the surroundings. The thermal resistance in this model is approximated using τ_{th}, the thermal time constant of natural cooling of the stack [49]

$$R_{th} = \frac{\tau_{th}}{C_{th}}\ . \tag{16}$$

Alternatively, the thermal admittance, h, is used to describe the heat loss

$$\dot{Q}_{loss} = h(T - T_{amb}) \tag{L2}$$

where h describes the heat transfer ability of the stack [57].

The cooling rate, $\dot{Q}_{cool}$, represents the amount of energy that the thermal management system of the electrolyzer must remove from the system to avoid overheating. Some models describe it with the coolant properties

Author	Generation	Loss	Thermal Cooling	Miscellaneous	Reference
Agbli et al.	G2	L1	TC1	—	[38]
Espinosa-Lopez et al.	G1	L1	not defined	M1	[47]
Fragiocomo et al.	G1	L1	not defined	—	[48]
Gabrielli et al.	G1	L1	TC2	—	[49]
Garcia-Valverde et al.	G1	L1	not defined	—	[50]
Grigoriev et al.	G1	—	TC2	—	[52]
Keller et al.	G1	L2	TC1	—	[54]
Lebbal et al.	G1	—	TC2	—	[57]
Ogumerem et al.	G1	—	—	M2	[64]
Olivier et al.	G1	L1	TC1	—	[66]
Schnuelle et al.	G1	L1	TC2	—	[75]
Sood et al.	G2	L1	—	—	[76]
Tabanjat et al.	G2	—	—	—	[77]
Zhang et al.	G2	—	TC1	—	[83]

Table 2: Thermal Models in Literature.

$$\dot{Q}_{cool} = \dot{m}_c c_{p,c}(T_c^{in} - T_c^{out}) \tag{TC1}$$

where $\dot{m}_c$ and $c_{p,c}$ are the coolant mass flow rate, and specific heat respectively, which are multiplied with the coolant temperature difference in, T_c^{in}, and out of the electrolyzer, T_c^{out}. The value of cooling can also be approximated using the logarithmic mean temperature difference (LMTD) method [49]. In most cases, water that flows through the anode and cathode cools the cell, so some models simplify the energy balance, Eq. (11), to a closed system equation

$$C_{th}\frac{dT}{dt} = \dot{Q}_{net} \tag{17}$$

and include the rate of energy from the water into and out of the system as heat rejected due to cooling

$$\dot{Q}_{cool} = \dot{m}^{in}_{H_2O} c_{p,H_2O} T^{in}_{H_2O} - \dot{m}^{out}_{H_2O} c_{p,H_2O} T^{out}_{H_2O} \,. \tag{TC2}$$

Other models acknowledge that thermal cooling is necessary once the target temperature is exceeded, but do not define the value of such cooling in their model [48].

Finally, the miscellaneous term can include models of pump heat generation

$$\dot{Q}_{pump} = \dot{V}\Delta P_{pump} - \dot{W}_{pump,elec} \tag{M1}$$

which quantifies the heat generated based on the difference in the pump work, quantified by the product of $\dot{V}$, the water flow rate, and ΔP_{pump}, the pump head needed, and the electrical work, $\dot{W}_{pump,elec}$ [47].

Another miscellaneous term describes the heat transfer from radiation

$$\dot{Q}_{rad} = A_s \epsilon \sigma (T^4 - T^4_{amb}) \tag{M2}$$

where the radiation from the body with a given surface area, A_s, surface emissivity, ϵ and surface temperature, T is described. In this equation, σ is the Stefan-Boltzmann constant [64].

The ODE thermal models introduced here are the popular choice for control systems design analysis, however some literature describes PDE thermal models [40, 65] which can be used for optimization [84, 85]. Such models are particularly important to evaluate inefficiencies in operation and foster a deeper understanding of the dynamics of the PEM water electrolyzer cell.

3.3. Mass Transport Models

Mass transport submodels describe the movement of chemical species within the cell and are employed to calculate concentrations and membrane properties such as gas crossover and water content. A comprehensive review of mass transport and fluid modeling is performed by Maier et al. [26], however, this section focuses on mass transport models that can be used in control design and analysis.

3.3.1. ODE Models for Mass Transport

The electrolysis reaction produces hydrogen and oxygen by splitting water. An ODE model for mass transport begins with quantifying this reaction, The molar production rate of hydrogen, $\dot{n}^p_{H_2}$, within the cathode half-reaction in Eq. (2) is related to the electrolyzer current density, i_{el}, and the number of cells in the electrolyzer stack, N_c, as follows [47]

$$\dot{n}^p_{H_2} = \frac{i_{el} N_c}{zF}\eta_F \,. \tag{18}$$

Using the reaction stoichiometry, the oxygen production, $\dot{n}^p_{O_2}$, and water production, $\dot{n}^p_{H_2O}$, in the anode are found as

$$\dot{n}^p_{O_2} = \frac{i_{el} N_c}{2zF}\eta_F \tag{19}$$

$$\dot{n}^p_{H_2O} = -\frac{i_{el} N_c}{zF}\eta_F \,. \tag{20}$$

The Faraday efficiency, η_F, accounts for all the electrons that are not involved in the electrolysis reaction; however, in some

Author	Type	H_2 Crossover	O_2 Crossover	Reference
Abdin et al.	ODE	—	—	[35]
Afshari et al.	ODE	G1 + G2 + G3	G1 + G3	[37]
Aubras et al.	ODE	—	—	[40]
Chandesris et al.	—	G4	G4	[43]
Espinosa et al.	ODE	—	—	[47]
Fragiacomo et al.	ODE	—	—	[48]
Gabrielli et al.	ODE	G1	negligible	[49]
Grigoriev et al.	PDE2	G4	G4	[52]
Grigoriev et al.	—	G1	G1	[86]
Kim et al.	PDE1	G1	negligible	[55]
Liso et al.	ODE	—	—	[59]
Moradi Nafchi et al.	ODE	—	—	[62]
Ogumerem et al.	ODE	—	—	[64]
Ojong et al.	PDE2	—	—	[65]
Olivier et al.	ODE	—	—	[66]
Sartory et al.	ODE	G1	G1	[70]
Schalenbach et al.	ODE	G1 + G2	G1	[72]
Schnuelle et al.	ODE	—	—	[75]
Shin et al.	ODE	—	—	[87]
Sood et al.	ODE	—	—	[76]
Tijani et al.	ODE	G1 + G2 + G3	G1 + G3	[78]
Trinke et al.	—	G1	—	[88, 89]
Yigit et al.	ODE	—	—	[82]
Zhao et al.	PDE3	—	—	[84, 85]

Table 3: Mass Transport Models in Literature.

cases it is assumed to be 100% [78]. Models of efficiency are discussed in a later section. The flow of these species within the electrolyzer are modeled in separate domains of the anode, cathode, and membrane.

Anode. Within the anode, water is split and oxygen forms. The instantaneous change in molar concentration of oxygen and water is computed using the conservation of mass

$$\frac{dn_{O_2}}{dt} = \dot{n}^{in}_{O_2} - \dot{n}^{out}_{O_2} + \dot{n}^{p}_{O_2} \tag{21}$$

$$\frac{dn_{H_2O}}{dt} = \dot{n}^{in}_{H_2O} - \dot{n}^{out}_{H_2O} - \dot{n}^{mem}_{H_2O} + \dot{n}^{p}_{H_2O} \tag{22}$$

where $\dot{n}^{in}_{O_2}$, $\dot{n}^{out}_{O_2}$ and $\dot{n}^{in}_{H_2O}$, $\dot{n}^{out}_{H_2O}$ are the anode inlet and outlet molar flow rates of oxygen and water, respectively, and $\dot{n}^{mem}_{H_2O}$ is the flow rate of water across the membrane [35].

Cathode. On the cathode side, hydrogen is formed and there is water crossover across the membrane, such that the balance of these species is given as

$$\frac{dn_{H_2}}{dt} = \dot{n}^{in}_{H_2} - \dot{n}^{out}_{H_2} + \dot{n}^{p}_{H_2} \tag{23}$$

$$\frac{dn_{H_2O}}{dt} = \dot{n}^{in}_{H_2O} - \dot{n}^{out}_{H_2O} + \dot{n}^{mem}_{H_2O} \tag{24}$$

where $\dot{n}^{in}_{H_2}$, $\dot{n}^{out}_{H_2}$ and $\dot{n}^{in}_{H_2O}$, $\dot{n}^{out}_{H_2O}$ are the cathode inlet and outlet molar flow rates of hydrogen and water, respectively [35].

Membrane. The total water that crosses the membrane is described in literature as the sum of 3 components as follows

$$\dot{n}^{mem}_{H_2O} = \dot{n}^{diff}_{H_2O} + \dot{n}^{eod}_{H_2O} - \dot{n}^{pe}_{H_2O} \tag{25}$$

where $\dot{n}^{diff}_{H_2O}$, and $\dot{n}^{eod}_{H_2O}$ are the molar flow rates of water due to diffusion and electro-osmotic drag from anode to cathode, and $\dot{n}^{pe}_{H_2O}$ is the flow rate from the hydraulic pressure effects from cathode to anode.

Diffusion of water across the membrane, derived by Abdin et al. [35], is calculated from Fick's law of diffusion

$$\dot{n}^{diff}_{H_2O} = \frac{AD_w}{\delta_{mem}}\Big(\Big[\frac{\rho_{H_2O}(T_{cat})}{M_{H_2O}} + \frac{\delta^{cat}_{el}\dot{n}^{cat}_{H_2O}}{D^{cat}_{eff}}\Big] - \Big[\frac{\rho_{H_2O}(T_{an})}{M_{H_2O}} - \frac{\delta^{an}_{el}\dot{n}^{an}_{H_2O}}{D^{an}_{eff}}\Big]\Big) \tag{26}$$

where A is the membrane area, D_w is the diffusion coefficient of water in the membrane, and M_{H_2O} is the molecular weight

of water. The value of δ_{mem} is the membrane thickness and δ_{el}^{cat} and δ_{el}^{an} are the thicknesses of the cathode and anode, respectively. The molar flux of water through the cathode, $\dot{n}_{H_2O}^{cat}$, describes the flow of water across the membrane from the anode and the molar flux of water through the anode, $\dot{n}_{H_2O}^{an}$, is the water consumed through the reaction and crossover to the cathode. Finally, D_{eff}^{cat} and D_{eff}^{an} are the effective binary diffusion coefficients of the cathode and anode, respectively [35].

Electro-osmotic drag is the dominant process which drives water transport across the membrane. It is directly related to the flux of protons migrating across the membrane and it is described as

$$\dot{n}_{H_2O}^{eod} = \frac{n_d I}{F} \tag{27}$$

where n_d is the electro-osmotic drag coefficient which is experimentally found to be non-constant.

Finally, the water transport as a result of the pressure gradient is described by Darcy's Law

$$\dot{n}_{H_2O}^{pe} = \frac{K_{Darcy} A \rho_{H_2O} \Delta P}{\delta_{mem} \mu_{H_2O} M_{H_2O}} \tag{28}$$

where K_{Darcy} is the membrane permeability and μ_{H_2O} is the dynamic viscosity of water [35].

These three terms describe the driving forces behind the flow of water across the membrane. Such models are critical to effective control design and deep understanding of PEM water electrolyzer operation.

3.3.2. PDE Models for Mass Transport

PDE mass transport submodels describe the flow of species in multiple dimensions, but with increased complexity. ODE models are used generally for design and analysis of control systems. However, some recent work from Zhao et al. [84, 85] uses PDE mass transport models for a more accurate simulation of mass transport in a cell. The simplest PDE models add a single dimension to the ODE models discussed above such that Eq. (21) becomes

$$\frac{\partial n_{O_2}}{\partial t} = \frac{\partial n_{O_2}}{\partial z} + \dot{n}_{O_2}^{p} \tag{PDE1}$$

in which ∂z represents an infinitesimal change in the transverse direction through the domain. The other equations follow the same pattern [55]. Other mass transport models describe the mass balance as

$$\frac{\partial C}{\partial t} + u \cdot \nabla C_i = \nabla \cdot (D_i \nabla C_i) + \dot{R}_i \tag{PDE2}$$

where C_i and D_i are the concentration and diffusion coefficients of the dissolved species, respectively [65]. The reaction term $\dot{R}_i$ is calculated with Faraday's Law.

Similarly, other models describe the mass flux of each species based on diffusion as

$$\dot{n}_i = -\frac{1}{RT}\Big(\frac{B_0 y_i P}{\mu}\nabla P - D_i^{eff}\nabla(y_i P)\Big) \tag{PDE3}$$

where B_0 is the permeability coefficient, y_i is the mole fraction, and D_i^{eff} is the effective diffusivity of each component i in the mixture [84, 85].

3.3.3. Gas Crossover

As the electrolysis reaction occurs, some of the oxygen forming in the anode and hydrogen forming in the cathode permeate across the membrane. Although this occurs at low rates, the hydrogen crossover phenomenon is important to model for safety concerns since the lower explosive limit is 4% molar hydrogen in oxygen [72].

The models characterized in Table 3 describe the terms included to model hydrogen and oxygen crossover. Note that Eq. (21) and (23) neglect gas crossover but these equations can be easily modified to include crossover. Gas crossover is driven by the following phenomenon: diffusion, pressure difference, and electro-osmotic drag.

To model the permeation of hydrogen and oxygen across the membrane based on diffusion, Grigoriev et al. [86] developed the following models

$$\dot{n}_{H_2}^{perm} = \varepsilon_{H_2}^{\text{diff}} \frac{P_{H_2,c} - P_{H_2,a}}{\delta_{mem}} A \tag{G1}$$

$$\dot{n}_{O_2}^{perm} = \varepsilon_{O_2}^{\text{diff}} \frac{P_{O_2,a} - P_{O_2,c}}{\delta_{mem}} A \tag{G1}$$

where $P_{H_2,c}$, and $P_{H_2,a}$ are the partial pressures of the hydrogen in the anode and cathode, respectively, while $P_{O_2,c}$, and $P_{O_2,a}$ are the partial pressures of the oxygen in the anode and cathode, respectively. $\varepsilon_{H_2}^{\text{diff}}$, the permeability coefficient of the hydrogen, is calculated with

$$\varepsilon_{H_2}^{\text{diff}} = \frac{D_{H_2}}{H_{H_2}} \tag{29}$$

where D_{H_2} is the diffusivity of hydrogen in the membrane and H_{H_2} is Henry's constant for hydrogen. $\varepsilon_{O_2}^{\text{diff}}$, the permeability coefficient of the hydrogen, is calculated with

$$\varepsilon_{O_2}^{\text{diff}} = \frac{D_{O_2}}{H_{O_2}} \tag{30}$$

where D_{O_2} is the diffusivity of oxygen in the membrane and H_{O_2} is Henry's constant for oxygen. Some models deem the oxygen crossover rate negligible as it is significantly lower than the hydrogen crossover rate and not a safety concern [55].

To increase the complexity, some models add a term to the hydrogen crossover rate that accounts for the hydrogen that is driven across the membrane by a difference in pressure from the anode to the cathode [72]

$$\dot{n}_{H_2}^{perm} = \varepsilon_{H_2}^{dp} \frac{P_{H_2,c} - P_{o_2,a}}{\delta_{mem}} A \tag{G2}$$

where $\varepsilon_{H_2}^{dp}$ describes the permeability of hydrogen based on the differential pressure.

While some models deem it negligible [72], others include a description of the hydrogen or oxygen crossover based on the effects of electro-osmotic drag [37]. This phenomenon is based

on the convection of the proton flow across the membrane and operates only in one direction as described by

$$\dot{n}_{H_2}^{perm} = -\frac{i_{el}}{F}\zeta\frac{P_{H_2,c}S_{H_2}}{C(H_2O)}A \tag{G3}$$

$$\dot{n}_{O_2}^{perm} = \frac{i_{el}}{F}\zeta\frac{P_{O_2,a}S_{O_2}}{C(H_2O)}A \tag{G3}$$

where $C(H_2O)$ is the concentration of water in the membrane and ζ is an experimentally determined drag coefficient based only on temperature

$$\zeta = 0.0134T + 0.03 \tag{31}$$

The solubility of the membrane for hydrogen, S_{H_2}, is described as

$$S_{H_2} = \frac{\varepsilon_{H_2}^{\text{diff}}}{D_{H_2}} \tag{32}$$

while the solubility of the membrane for oxygen, S_{O_2}, is described as

$$S_{O_2} = \frac{\varepsilon_{O_2}^{\text{diff}}}{D_{O_2}} \tag{33}$$

In PDE models, the crossover based on diffusion and electro-osmotic drag is described as

$$v_{H_2O} \cdot \nabla C_i = \nabla \cdot (D_i \nabla C_i) \tag{G4}$$

where v_{H_2O} is the velocity of water through the membrane, while the concentration, C_i, and diffusivity, D_i are described for the given species i [43].

This concludes the complex submodeling of PEM WEs, however, simple empirical models such as equivalent circuit models are often employed when computational time is more important than accuracy. The next section describes equivalent circuit models for water electrolysis.

3.4. Equivalent Circuit Models

The simplest of PEM WE models are based on experimentally derived empirical parameters that allow the operation of a WE to be simplified into a well studied concept. Equivalent circuit models describe the cell dynamics with electrical components.

3.4.1. Static

The simplest models of a PEM water electrolyzer employ a static equivalent circuit to describe the operation of the stack with a resistor in series with a reversible voltage. This is based on a linear approximation of the current-voltage (I-V) characteristic curve in which V_{int} represents the critical voltage for which the current flow starts and the slope is described with the resistor, R_i, that represents the irreversibilities in the cell. The static equivalent circuit is shown in Fig. 4 from Atlam and Kohle [90].

The voltage of the electrolyzer cell is computed as

$$V_{cell} = i_{el}R_i + V_{int} \tag{34}$$

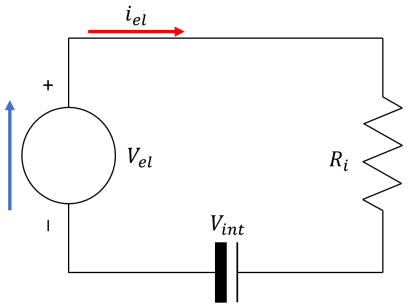

Figure 4: Static Equivalent Circuit recreated from Atlam and Kohle [90].

where the variation of cell resistance with respect to pressure and temperature takes the form

$$R_i = R_0 + kln\left(\frac{p}{p_0}\right) + dR_t(T - T_0) \tag{O3}$$

where R_0, p_0, and T_0 are the reference resistance, pressure, and temperature, respectively. The curve fitting parameter, k, and the resistance coefficient of temperature, dR_t, are empirically derived from the I-V characteristics of a PEM WE cell measured at various temperatures and pressures [90, 91].

The static equivalent circuit models, although effective in computing the static value of voltage, cannot predict the voltage variation during transient operation, and thus effective dynamic models are necessary to simulate a cell's voltage during non steady-state conditions.

3.4.2. Dynamic

A dynamic model recreated from Guilbert and Vitale [92] is shown in Fig. 5. This model uses both resistor and capacitor elements to simulate the anode and cathode. As before, the membrane is modeled with a simple resistor.

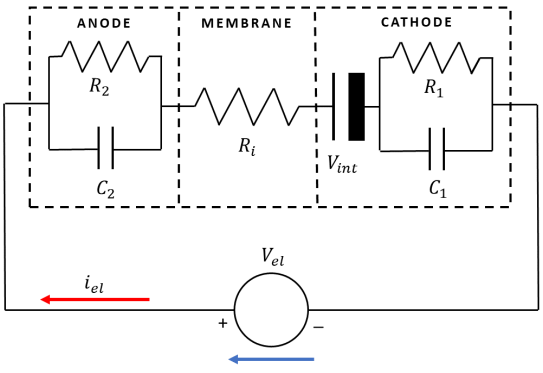

Figure 5: Dynamic Equivalent Circuit recreated from Guilbert and Vitale [92].

This model describes the electrolyzer voltage as the sum of the reversible potential and the ohmic and activation overpotentials [93, 94, 95, 96]

$$V_{cell} = V_{act,a} + i_{el}R_i + V_{int} + V_{ohm} + V_{act,c} \tag{35}$$

Based on the equivalent circuit, the RC cells describe the following dynamic relationship for the activation overpotentials of the anode and cathode

$$\frac{dV_{act,a}}{dt} = \frac{1}{C_2} i_{el} - \frac{1}{R_2 C_2} V_{act,a} \tag{36}$$

$$\frac{dV_{act,c}}{dt} = \frac{1}{C_1} i_{el} - \frac{1}{R_1 C_1} V_{act,c} \tag{37}$$

where RC represents the time constant of a system [20].

Figure 6 compares the response of the dynamic equivalent circuit by Guilbert and Vitale [92] to the static equivalent circuit model and the experimental results for two steps in the cell voltage. As seen, the dynamic model can predict the cell voltage during transient operation with reasonable accuracy.

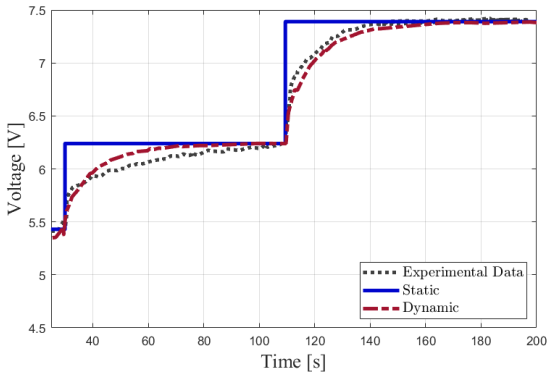

Figure 6: Experimental Data Compared with Static and Dynamic Equivalent Circuit Models Recreated from Guilbert and Vitale [92].

With experimentally derived parameters, equivalent circuit models can effectively capture the voltage dynamics of a water electrolyzer. However, for most applications, only predicting the voltage dynamics is not enough and modeling other cell operating parameters such as temperature and concentration of different species is necessary to ensure an efficient, safe, and durable cell operation.

3.5. Degradation Modeling

Modeling and analysis of the rate and mechanisms of PEM WE degradation in different conditions enable control designs that prolong the stack life. The review of degradation by Feng et al. [97] thoroughly details the sources of degradation on various cell components, which include membrane degradation from chemical thinning [43, 98], pollution [99], and thermal degradation [43, 100]. The electrodes can also see degradation from the harsh electrochemical environment on the anode [101] and titanium corrosion from dynamic operation [102].

While there has been some research into degradation models for fuel cells [103, 104, 105], there are very few models that have been developed to quantify and analyze degradation in electrolyzers. Most PEM WE modeling attempts acknowledge that degradation can be caused by malicious dynamic operation and high temperature, which can be mitigated by control design, but they don't include a model which quantifies the degradation rate. Only Chandesris et al. [43] have created a model which describes the chemical degradation leading to fluoride release and thinning of the cell membrane. The change in membrane thickness is described as

$$\frac{d\delta_{mem}}{dt} = \Delta\delta_{mem} \dot{n}_{fluor} \tag{38}$$

where $\Delta\delta_{mem}$ describes the membrane thinning per mole of fluoride released and $\dot{n}_{fluor}$ is the rate of fluoride released. The model analyzed the thickness of the membrane over time, noting an increase of oxygen crossover between the anode and cathode as the membrane thinned, as well as formation of Fe radicals at the cathodic side due to system impurities.

3.6. Electrolyzer Efficiency

To understand the operation of a PEM WE from a systems engineering perspective, the most important parameter is the efficiency. The total energy efficiency of the cell, η_{el}, can be described with the product of several distinct efficiencies

$$\eta_{el} = \eta_V \eta_F \eta_C \tag{39}$$

in which η_V is the voltage efficiency, η_F is the Faraday efficiency, and η_C is the compression efficiency.

The voltage efficiency η_V, represents the difference between the ideal reversible voltage, V_{rev}, and the actual cell voltage, V_{cell} as calculated in the electrochemical model [72]

$$\eta_V = \frac{V_{rev}}{V_{cell}} . \tag{40}$$

The maximum value of the voltage efficiency is based on the amount of chemical energy obtained from the reaction compared to the ideal energy supplied to the cell. The chemical energy obtained is described by the lower heating value of hydrogen, H_{LHV}, and the ideal energy corresponding to the thermoneutral voltage, V_{th}, such that

$$\eta_{V_{max}} = \frac{\frac{H_{LHV}}{2F}}{\frac{\Delta G + T\Delta S}{2F}} = \frac{\frac{H_{LHV}}{2F}}{V_{th}} \approx 84.6\% \tag{41}$$

which is the approximately 84.6 % [74].

The Faraday efficiency, η_F, instead compares the ideal charge for a given hydrogen production volume, Q_{id}, to the real charge, Q_{re}

$$\eta_F = \frac{Q_{id}}{Q_{re}} . \tag{42}$$

An empirical model derived by Yodwong et al. [106] describes the Faraday efficiency as

$$\eta_F = a\left(\frac{i_{el}}{A}\right)^b + c \tag{43}$$

in which A is the cross sectional area and a is a linear function of pressure, while b and c are empirically found to be constants of -1 and 1, respectively.

Schalenbach et al. [72] instead relate the Faraday efficiency to the gas crossover of both hydrogen and oxygen

$$\eta_F = 1 - 2F\frac{\dot{n}^{perm}_{H_2}}{i_{el}A} - 4F\frac{\dot{n}^{perm}_{O_2}}{i_{el}A} \tag{44}$$

as any gas permeating the membrane is not included in the products of the reaction and exposes the decrease in efficiency.

Often, the hydrogen from a water electrolyzer is compressed to create a more dense form of energy storage, so Scheepers et al. [73, 74] include the compression efficiency, η_C, which is based on the work required for each compression stage.

An example of the efficiencies for a PEM WE at various current densities are displayed in Fig. 7 with curves recreated from Tijani et al. [78] and Scheepers et al. [74].

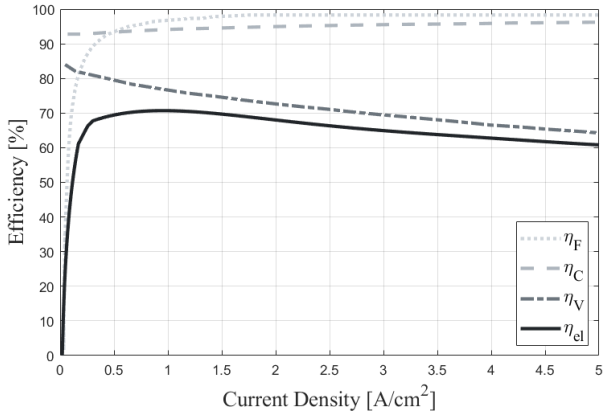

Figure 7: An Example of PEM WE Efficiency Curves Recreated from Tijani et al. [78] and Scheepers et al. [74]. Includes Faraday, Compression, Voltage, and Total Efficiency.

This concludes the description and categorization of PEM electrolyzer modeling. Control system development relies on accurate but simple models that can emulate the system dynamic response quickly. However, this classification exposes a gap between simple equivalent circuit models that produce minimum information about different operating parameters and detailed complex models that accurately model the processes within a cell and require knowledge of many hard-to-access parameters to produce accurate results. Control system design benefits from models that match the operation but require limited complexity and computational power. Simplification of detailed models, specifically by adding data-driven components can address this gap to produce simple but effective control-oriented models.

4. System Control

A suitable control system can maximize the performance and life-cycle of a PEM WE system given the current state-of-the-art in materials and stack design. In this section, we discuss various control related challenges for PEM WE operation, the available controllable system variables and knobs, their impact on system operation, and different controller design methodologies adopted in literature.

4.1. System Challenges and Variables

The different applications of water electrolyzers discussed so far pose unique operational challenges for the system. The key control challenges for PEM WEs can be traced to the system physics and can be associated with particular system variables.

4.1.1. Stack Voltage

PEM WE stacks are highly sensitive to the terminal voltage at which they operate. High over-voltages lead to increased catalyst loss and degradation, while low voltages can not activate the electro-catalytic breakdown [107]. Moreover, the relatively low terminal voltage of electrolyzers means that any coupling with renewable energy systems or the electric grid must be done through step-down converters. Since the voltage output of RES like PV systems or wind turbines is highly transient, active control of the step-down converters is needed to maximise operating efficiency for the entire green hydrogen production system. Bernt et al. [108] also noted that intermittent power supply with cycling to and from the open circuit voltage resulted in accelerated iridium loss and increased contact resistance in the anode.

The studies that focus on actuating the stack terminal voltage gain secondary control over other system variables like current density, power consumption, and hydrogen production rate through the system physics [109, 85, 110, 66, 84, 94]. As an example, Zhao et al. [84] defined the primary performance criterion with respect to the system voltage slew rate. They improved the performance by breaking a single voltage ramp into two segments and optimising the rate and duration of each segment. It is to be noted that critical system characteristics like local reactant starvation are highly sensitive to the rate of voltage change and the sustained duration. So, a direct control over the stack voltage can potentially aid stack life management.

4.1.2. Stack Current Density

Current density is a critical system parameter for PEM WE operation. The hydrogen production rate of the stack is directly proportional to the current density and other key system variables like hydrogen crossover rate, Faradaic efficiency, and even voltage degradation depend on it, making it a widely studied control knob in literature [111, 112, 113, 114, 115, 93]. As mentioned, the hydrogen in oxygen volume fraction in the anode should not exceed the lower flammability limit of 4% volume-in-volume. The system controller must maintain the electrolyzer stack above the critical current density even when supplied with low electric input power from an RES [37]. Else, the electrolyzer must shut down to preserve safety of the system and its operators. The critical current density value is dependent on the membrane thickness, pressure difference, and temperature [88]. Therefore, current density needs to be regulated for safe electrolyzer operation. System efficiency and health are other reasons to regulate the stack current due to the strong dependence of voltage degradation [116] and hydrogen crossover [72], and consequently Faradaic efficiency, on the current density.

Apart from the absolute value, rapid changes in current density have also been shown to be detrimental to electrolyzer components such that commercial stacks often have encoded

restrictions on current slew rates [114]. Ruuskanen et al. [117] have shown the detrimental effects of current ripple on alkaline electrolyzer efficiency, highlighting the need for better power electronics control of input electrical energy, which might be relevant for PEM electrolyzers as well. Guilbert et al. [94] have argued that the input current harmonics lead to increased ionic vibrations and consequently efficiency loss. Weiss et al. [98] found that repeated cycling between operation and rest led to enhanced Iridium dissolution from the anode active sites and thus increased stack degradation.

However, Frensch et al. [118] observed reduction in terminal voltage over time, when the PEM WE was supplied with cyclic load profile. This suggests some advantage to the transient component of power supply. The degradation behaviour also varied with change in the period of the cyclic load profile. While a period of 10s reduced the terminal voltage over time, a period of 100s led to voltage degradation. The transient characteristics of the power supply influence the oxygen bubble dwell time in the anode porous transport layer, which has been linked to increased Ti-passivization, causing a permanent increase in ohmic overpotential. Clearly, the impact of current transience is dependent on its frequency, duration, and severity. A comparative study on the real-time and long-term effects of these different aspects of transient power supply can shed more light on this matter.

4.1.3. Feedwater Flow Rate

Since water is the only physical input to a water electrolyzer, feedwater flow rate has a deep influence on its operation, through phenomena like bubble formation and coverage, and reactant starvation [119]. Modeling the overpotential due to bubble coverage as a hindrance to electron and ion transport inside the stack is presented in the Bubble Overpotential section through Eq. (10) - (B3). Higher fidelity bubble modeling have been developed by Ojong et al. [65] and Aubras et al. [40]. Interestingly, Garcia et al. [120] have shown the impact of water flow rate on bubble size at relevant flow rate regimes to be negligible. Further studies need to be done to study the interdependence of feedwater flow rate, bubble coverage, current density, and stack efficiency. The influence of feedwater flow rate on the stack terminal voltage is further clarified in the work of Ogumerem et al. [64], who used the flow rate to keep stack voltage below the 2V threshold, in the face of system disturbance in the form of changing stack current density. Apart from bubble coverage, water flow rate impacts stack safety as well. Critically low feedwater flow rates causes irreversible damage to the stack by creating local hot-spots of increased current density and temperature as shown by Immerz et al. [121].

Feedwater mass flow rate control has been used to manipulate the hydrogen production rate in multiple studies, as it supplies the essential reactant for the electrolysis process [122]. In addition to bubble coverage regulation, optimum water flow rate controllers can increase hydrogen production, reduce water usage and electrical power requirement from water pumps, conditioning units, and filtration systems. Reducing water usage might be of greater concern for projects considering electrolyzer operation coupled to off-shore wind turbines or in marine environments, where water desalination imposes a high energy cost on the entire system [123, 124].

4.1.4. Feedwater Temperature

Stack temperature plays a critical role in operating efficiency, and stack degradation. This is evident from Eq. (34) - (O3), where temperature is shown to have an effect on almost every aspect of the polarisation curve of an electrolyzer. It is also seen that the hydrogen crossover rate and hydrogen in oxygen volume fraction in the anode increase with temperature, especially at low current density ranges [88]. This is also apparent from the models of diffusion presented by Zhao et al. [84, 85], and summarised in Eq. (PDE3). It can thus be seen that feedwater temperature control can improve the stack safety, Faraday efficiency and current controllability at lower current ranges, which can be typical of power supply from solar photovoltaic systems on cloudy days [114, 17]. In electrolyzers, with adequate flow of water the stack temperature closely follows the feed water temperature. As an example, Tabanjat et al. [77] used feedwater temperature control to obtain a desired hydrogen production rate and Keller et al. [54] used heating elements and heat exchangers on the feedwater pipes to control the heat flow into the system and maintain the optimum stack temperature. Nevertheless, many studies did not consider the thermal dynamics in modeling or control design, citing the slower thermal response time compared to the electrochemical or even mass-transport dynamics.

4.1.5. Stack Pressure

Pressurized operation of PEM WEs is often pursued to lower the energy required by down-the-line balance of plant components such as mechanical compressors and gas drying systems that are necessary for hydrogen storage [125, 72]. The comparison between the efficiency of mechanical compression with electrolyzer operation at ambient conditions, and electrochemical compression in the cathode by asymmetric electrolyzer operation, has been the focus of various studies [125, 72, 126]. Controlling the cathode exit pressure provides an opportunity to dynamically change the operation mode and to crank the mechanical compression power up or down, to meet demand-side pressure requirements, in addition to optimizing the system efficiency and current controllability or dynamic range goals [88, 37, 89, 127, 114, 108]. However, increased cathode pressure leads to increased hydrogen diffusion to the anode side, increasing flamability risks. This can be counterbalanced by increasing the current density, as the dissolved hydrogen crosses back from the anode by electro-osmotic diffusion, as explained in Section 3.3. Trinke et al. [88] showed that hydrogen in oxygen volume fraction in the anode reduces upon increasing the current density. Thus, for safe electrolyzer operation, there exists a minimum current density at every pressure level. Increasing the cathode exit pressure increases the current cut-off value, thereby restricting the operating window and degrading the current controllability of the stack. Koponen et al. [114] found this

Algorithms \ Variables	Stack Voltage	Current Density	Water Flowrate	Stack Temperature	System Power Control
Feedforward	[94]	—	[122]	[54]	—
PI/PID Controllers	[110, 66]	[115, 112, 66, 113, 115]	—	[54]	[128]
Optimal Control	[109, 85]	—	[64]	—	[129]
Fuzzy Logic	—	—	—	[77]	[130, 131]
Non-Linear Control	—	[93, 132]	—	—	—
Neural Networks	[85]	—	—	—	—

Table 4: Controller Algorithms and Controlled Variables Popularity.

to be critical for continuous stack operation on cloudy days for solar PV coupled electrolyzers which are characterized by sudden drops in electrical power supply. Since the cathode pressure influences hydrogen crossover, it is also crucial in regulating the Faraday and total efficiencies of the stack [70]. Comparatively, anode-side pressure, which is equal to the feedwater pressure, has a smaller effect on stack operating efficiency, as found by Toghyani et al. [81]. Nevertheless, pressurizing the anode can reduce pressure asymmetry, thereby increasing the Faraday efficiency and dynamic range of the stack.

4.2. Control Methods

The operational challenges of PEM WEs need to be managed properly to ensure an adequate performance while maintaining high system efficiency and long stack life. Apart from choosing the suitable variables to manipulate, the controller algorithm also plays a pivotal role in realizing the target performance. These choices are dependent on the unique challenges, needs and constraints of each application scenario. Table 4 outlines the different choices found in the published literature. It is seen that control design for stack voltage and current are addressed in literature more often, while PID controllers have often been used to benchmark more advanced control algorithms. In this section, we discuss different control algorithms adopted in literature to achieve the desired performance metrics. A direct comparison of the methods is not realistic due to the vast variety in system architecture and controlled parameters in different efforts.

4.2.1. Traditional Control Techniques

Dahbi et al. [122] implemented a feedforward control algorithm for the feedwater flow rate, based on an optimal flow rate value derived as

$$\dot{m}^{in}_{H_2O} = \frac{9MP_{elec}}{nFV_{th}}\eta_F \tag{45}$$

where, $\dot{m}^{in}_{H_2O}$ is the feedwater mass flow rate, P_{elec} is the electrical power delivered to the electrolyzer stack, η_F is the Faraday efficiency, n is the number of electrons formed per mole of product, M is the molar mass of hydrogen, F is the Faraday constant, and V_{th} is the thermoneutral voltage as desribed in Eq. (14). It was found that hydrogen production rate and thus the stack efficiency is maximised for optimum water flow rate.

When compared to feedforward controllers, feedback controllers provide better disturbance rejection capabilities and are more robust in the face of variable system parameters. Hence, many studies have implemented proportional-integral-derivative (PID) controllers, with some variations to suit their particular application requirements [112, 115, 110, 128, 111, 113, 66, 54]. Among these, Proportional-Integral (PI) controllers are a simple and popular approach to produce the desired dynamic response and remove any steady-state error or offset. Many studies implemented PI controllers, for example to control the output current of DC-DC converters, which is equal to the stack current [112, 115, 110, 128]. Garrigos et al. [112] implemented a PI controller for the inner current control loop of a DC-DC converter to track the reference signal faster and cancel steady-state errors. Since the input voltage from RES can vary with multiple environmental and load factors, Guida et al. [115] gain scheduled the proportional gain of a PI controller to control the stack current with consistent dynamic performance across all operating points. Keow et al. [110] implemented online auto-tuning in addition to gain scheduling to actuate the stack voltage. The authors showed that while online auto-tuning of the controller provides a consistent performance over changing system parameters, due to degradation and other model uncertainties, gain scheduling reduces the frequency of such auto-tune exercises. The gain scheduling was a critical part of their method because the authors used a model-free tuning approach in their work. In systems having electrolyzers coupled to RES for green hydrogen production, or as a variable on-demand load, maintaining the power quality supplied to the grid is of prime importance. Hence, Chiesa et al. [111] used low gain integral controllers along with high pass filters to reduce noise propagation through the current actuation. The authors also implemented a droop control function to further decrease the voltage fluctuations. Kim et al. [128] developed a system with fuel cells and electrolyzers to balance and stabilize a wind turbine power generation system. The inherent smooth power output provided by the PI controller was leveraged to generate stable reference power levels for the DC-DC converters controlling the operating points of the electrolyzer and fuel cell respectively. Voltage oscillations in response to sudden changes in wind speed were further reduced with the use of droop control.

Using a derivative control element in addition to the proportional and integral components improves dynamic reference tracking [113]. Thus, Olivier et al. [66] adopted a PID controller to track a hydrogen production rate set-point by manipulating the stack voltage. This control system also applied a logic-based ON-OFF regulation of stack temperature, and water levels in the oxygen and hydrogen separator vessels. Keller et al. [54] implemented a gain scheduled PID controller with a model-based feedforward component to reject deviations resulting from model uncertainties. In their work, the operating point dependent PID parameters provided consistent dynamic range across the entire operating window. In order to smoothen the control input, the authors deployed the following parameter transition function

$$K_s(t) = (1 - \alpha(t))K_{S-old} + \alpha(t)K_{S-new} \tag{46}$$

where K_{S-old} and K_{S-new} are the system amplification parameters from previous and new operating conditions, and $\alpha(t)$ is given by

$$\alpha(t) = tanh(kr(t))$$

where $r(t)$ signifies a time dependent ramp rising from 0 to 1 as the operating condition changes and k defines the slope.

4.2.2. Optimal Control Techniques

To improve the efficiency of electrolyzer operation and produce hydrogen at a lower cost, many researchers have investigated optimal control techniques [64, 85, 129]. Gabrielli et al. [49] employed mixed-integer linear programming (MILP) for optimizing the day-long operation of a PEM electrolyzer and fuel cell separately. For the electrolyzer, the algorithm minimized the production cost of a given hydrogen volume over a day, with variable electricity prices. The cost function to be minimized was given as

$$\min_{P,\delta} \sum_{t=1}^{N} p[t](P[t] + \gamma\delta[t]) \tag{47}$$

subject to

$$\begin{aligned} V^S[t+1] &= V^S[t] + V(P[t]) \\ T[t+1] &= \alpha T[t] + \beta' \\ T[t] &<= T_{max} \\ 0 <= P[t] &<= P_{max}\delta[t] \\ V^S[t] >= 0, V^S[0] &= 0, V^S[N] = V_N^S, T[0] = T_0 \end{aligned}$$

where, V is the volume of hydrogen, with S representing storage, P is electrical power, p is electricity price, γ is the balance of plant power consumption, δ is the binary variable indicating ON/OFF state of the device, T is temperature, α and β are temperature evolution constants, t is the time-step, and N is the total number of time-steps. While comparing the performance of the algorithm on a linear and a piecewise affine efficiency model, the authors found the linear model to under-estimate hydrogen production and over-estimate hydrogen consumption.

A model predictive control (MPC) algorithm finds the control law by iteratively solving an optimization problem over a receding horizon. MPC is a strong tool to achieve an optimal performance without violating system constraints, which are critical for safe operation of a WE. However, for practical applications, MPC is computationally expensive for systems with complex models, such as a multi-physics model for a PEM WE. Therefore, Flamm et al. [129] used piece-wise affine approximations to model an electrolyzer to be used within an MPC controller that produces hydrogen at minimum cost from a combination of PV and grid power supplies. In another work, Ogumerem et al. [64] developed a multi-parametric model predictive controller to regulate the stack temperature by actuating the feed water flow rate. The controller was designed to keep the stack terminal voltage below a pre-defined threshold while rejecting system disturbance in the form of changes in stack current, which represented a change in the hydrogen production rate. While MPC optimization problems need to be solved at every time-step, the authors solved the optimization problem once to obtain a set of parametric affine functions defining the optimal control input, using the PAROC framework [133]. The model used for prediction was also reduced into a simplified linear state-space system from the set of non-linear physics based equations. Fig. 8 shows the closed loop architecture used by the authors. They were able to reduce the computational requirements of their controller while achieving good target following and very low power consumption.

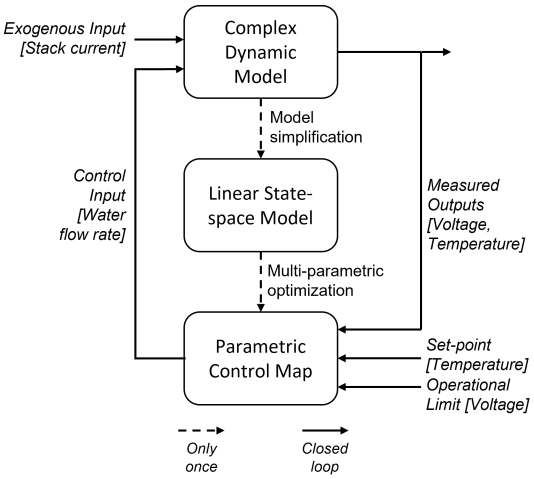

Figure 8: Optimal Control Architecture Adopted by Ogumerem et al. [64].

Developing physics-based models to be used with optimal and model predictive controllers requires rigorous modeling effort, and the resulting optimization problem can be complex to solve. To address this problem, Zhao et al. [85] used a neural network to model an electrolyzer system within a model predictive controller. The neural network replaces a complex non-linear plant model, thereby reducing computational cost of the MPC. The authors compared their MPC with an adaptive PID controller, in which the gains are determined by Fuzzy Logic. For the predictive controller, the authors defined the cost func-

tion as

$$J = \Sigma_{j=1}^{N_p}[P_{re}(k+j) - P_m(k+j)]^2 + \rho\Sigma_{j=1}^{N_c}[u_m(k+j-1) - u_m(k+j-2)]^2 \quad (48)$$

where, J is the cost function to be optimized, N_p is the prediction horizon, N_c is the control horizon, k is the current time-step, ρ is the weighting factor, P_m is the predictive model output, P_{re} is the reference output, and P_m is the predictive model output. The Neural network predictive controller was able to reduce the overshoot in response to step changes in supplied power by up to 92%. The reason for the better performance of the MPC controller can be traced down to the inherent advantage of MPC over PID control.

4.2.3. Other Controllers

Neural networks, fuzzy logic, and non-linear control algorithms were some of the other controllers seen in literature. Fuzzy Logic Controllers have been used widely in control and management of water electrolyzers, either to determine a set-point value or to generate gain values for traditional controllers. Tabanjat et al. [77] devised a PV-coupled electrolyzer system, where the electrolyzer feed water was used to cool the PV panel. A 2D FLC determined the water temperature set-point based on the difference in hydrogen production between reference and current temperature, and at successive time-steps. A PI controller was then used to follow the generated water temperature reference by actuating the cooling circuit pump. By exploiting the positive correlation between hydrogen production and stack temperature, this method increased hydrogen production by 56%. FLC was also used by Cano et al. [130] to generate the power input reference for both an electrolyzer and a fuel cell in a hybrid renewable energy system. They used stochastic models for the power demand and generation, to take into account the uncertainty with any prediction. A normal distribution was used to define the net power as

$$P_{net}(k) = N(\mu_{net}(k), \sigma^2_{net}(k)) \quad (49)$$

where, $\mu_{net}(k)$ and $\sigma^2_{net}(k)$ are the expected net power and the corresponding variance at time k given by

$$\mu_{net}(k) = \mu_{PV}(k) + \mu_{WT}(k) - \mu_L(k) \quad (50)$$

$$\sigma^2_{net}(k) = \sigma^2_{PV}(k) + \sigma^2_{WT}(k) + \sigma^2_L(k) \quad (51)$$

where, the subscripts PV, WT, and L stand for photovoltaic, wind turbine, and load respectively. The authors used current net power, the predicted change in net power, the variance of the prediction, and the state of charge (SOC) of the hydrogen storage system as input variables for the FLC. Their method was able to minimize start-stops for both the electrolyzer and fuel cell across all seasons, thereby reducing system degradation, while keeping the hydrogen storage in the desired SOC range.

The application of advanced non-linear control methods to water electrolyzers has been very limited. Guilbert et al. [93] implemented indirect sliding mode control (SMC) for manipulating the duty cycle of the Pulse Width Modulator for the DC-DC converter, where the sliding surface was given as

$$s = i_{el} - I_{el,ref} + K_i \int (i_{el} - I_{el,ref})dt \quad (52)$$

where, $i_{el} = i_2 - I_{C2} \approx i_2$, with the reaching law

$$\dot{s} = -\lambda s \quad (53)$$

where i_{el} is the electrolyzer stack current, $I_{el,ref}$ is the desired stack current, i_2 is the current through the secondary inductor, I_{C2} is the current through the secondary capacitor, and λ.

Sankar et al [132] used SMC to control a PEM fuel cell coupled to water electrolyzer. They implemented the SMC on the fuel cell to control power production by regulating the fuel flow rate, stack temperature, and air flow rate. Thus, the SMC for the fuel cell also sets the hydrogen production reference point for the electrolyzer. The SMC for the electrolyzer adhere to this, by actuating the stack current, while stack temperature is maintained by a separate PI controller. The authors studied the performance of the designed controller when used along with different nonlinear state observers for the fuel cell, of which the sliding mode observer provided best results. Although this study focused primarily on fuel cell control, the SMC implemented on the electrolyzer could be further studied for comparative performance of different state estimators on the electrolyzer control.

5. Conclusion

In this paper, we presented a detailed review of PEM water electrolyzer models relevant to control development, discussed their operational challenges and their connection to the system physics, and summarized different control methods adopted in literature to address these issues. We discussed both multi-physics models that fully describe interconnections between electrochemical, thermal, and mass transport submodels, and simple equivalent circuit models that can only estimate the cell voltage and current without access to internal cell variables or activities. It was noted that there is a gap for computationally efficient control-oriented models that also provide insight into the electrochemical and mass transport processes without the complexity of existing multi-physics models. Data-driven models are one of the possible pathways to arrive at such novel modeling framework.

The control design for water electrolyzers has mostly focused on single-input-single-output methods. Due to the complex interdependencies of different system variables in a PEM electrolyzer, multiple-input-multiple-output controllers can be beneficial from an efficiency and performance perspective. In addition, the highly non-linear nature of the plant calls for greater exploration of non-linear controllers. The difficulty in parameter identification for multi-physics models points toward greater uptake of data-driven and adaptive controller design methods.

Finally, while PEM electrolyzers have a quick dynamic response, it is shown that direct coupling with intermittent RES reduces the stack life and operating efficiency. Although well-designed controllers can mitigate the transiency in system variables to some degree, still more development in understanding the degradation mechanisms, models, and degradation-aware control algorithms is necessary.

References

[1] S. Griffiths, B. K. Sovacool, J. Kim, M. Bazilian, J. M. Uratani, Industrial decarbonization via hydrogen: A critical and systematic review of developments, socio-technical systems and policy options, Energy Research & Social Science 80 (2021) 102208.

[2] A. M. Oliveira, R. R. Beswick, Y. Yan, A green hydrogen economy for a renewable energy society, Current Opinion in Chemical Engineering 33 (2021) 100701.

[3] S. Evangelopoulou, A. De Vita, G. Zazias, P. Capros, Energy system modelling of carbon-neutral hydrogen as an enabler of sectoral integration within a decarbonization pathway, Energies 12 (13) (2019) 2551.

[4] M. Oertel, J. Schmitz, W. Weirich, D. Jendryssek-Neumann, R. Schulten, Steam reforming of natural gas with intergrated hydrogen separation for hydrogen production, Chemical engineering & technology 10 (1) (1987) 248–255.

[5] A. Boretti, B. K. Banik, Advances in hydrogen production from natural gas reforming, Advanced Energy and Sustainability Research 2 (11) (2021) 2100097.

[6] E. P. A. United States, Fast facts on transportation greenhouse gas emissions, `https://www.epa.gov/greenvehicles/fast-facts-transportation-greenhouse-gas-emissions/`.

[7] W. Liu, H. Zuo, J. Wang, Q. Xue, B. Ren, F. Yang, The production and application of hydrogen in steel industry, International Journal of Hydrogen Energy 46 (17) (2021) 10548–10569.

[8] O. B. Inal, B. Zincir, C. Deniz, Investigation on the decarbonization of shipping: An approach to hydrogen and ammonia, International Journal of Hydrogen Energy 47 (45) (2022) 19888–19900.

[9] C. Cunanan, M.-K. Tran, Y. Lee, S. Kwok, V. Leung, M. Fowler, A review of heavy-duty vehicle powertrain technologies: Diesel engine vehicles, battery electric vehicles, and hydrogen fuel cell electric vehicles, Clean Technologies 3 (2) (2021) 474–489.

[10] D. Verstraete, Long range transport aircraft using hydrogen fuel, International Journal of Hydrogen Energy 38 (34) (2013) 14824–14831.

[11] P. Lott, U. Wagner, T. Koch, O. Deutschmann, Hydrogen combustion engines–chances and challenges on the way towards a decarbonized mobility, Chemie Ingenieur Technik 94 (3) (2022) 217–229.

[12] P. Chiesa, G. Lozza, L. Mazzocchi, Using hydrogen as gas turbine fuel, J. Eng. Gas Turbines Power 127 (1) (2005) 73–80.

[13] F. Grueger, O. Hoch, J. Hartmann, M. Robinius, D. Stolten, Optimized electrolyzer operation: Employing forecasts of wind energy availability, hydrogen demand, and electricity prices, International Journal of Hydrogen Energy 44 (9) (2019) 4387–4397.

[14] R. Clarke, S. Giddey, F. Ciacchi, S. Badwal, B. Paul, J. Andrews, Direct coupling of an electrolyser to a solar pv system for generating hydrogen, International journal of hydrogen energy 34 (6) (2009) 2531–2542.

[15] B. Laoun, A. Khellaf, M. W. Naceur, A. M. Kannan, Modeling of solar photovoltaic-polymer electrolyte membrane electrolyzer direct coupling for hydrogen generation, international journal of hydrogen energy 41 (24) (2016) 10120–10135.

[16] A. Mraoui, B. Benyoucef, L. Hassaine, Experiment and simulation of electrolytic hydrogen production: case study of photovoltaic-electrolyzer direct connection, International Journal of Hydrogen Energy 43 (6) (2018) 3441–3450.

[17] A. Kosonen, J. Koponen, K. Huoman, J. Ahola, V. Ruuskanen, T. Ahonen, T. Graf, Optimization strategies of pem electrolyser as part of solar pv system, in: 2016 18th European Conference on Power Electronics and Applications (EPE'16 ECCE Europe), IEEE, 2016, pp. 1–10.

[18] A. Ibáñez-Rioja, P. Puranen, L. Järvinen, A. Kosonen, V. Ruuskanen, J. Ahola, J. Koponen, Simulation methodology for an off-grid solar–battery–water electrolyzer plant: Simultaneous optimization of component capacities and system control, Applied Energy 307 (2022) 118157.

[19] Z. Su, S. Ding, Z. Gan, X. Yang, Optimization and sensitivity analysis of a photovoltaic-electrolyser direct-coupling system in beijing, International journal of hydrogen energy 39 (14) (2014) 7202–7215.

[20] B. Yodwong, D. Guilbert, M. Phattanasak, W. Kaewmanee, M. Hinaje, G. Vitale, Proton exchange membrane electrolyzer modeling for power electronics control: a short review, C 6 (2) (2020) 29.

[21] Á. Hernández-Gómez, V. Ramirez, D. Guilbert, Investigation of pem electrolyzer modeling: Electrical domain, efficiency, and specific energy consumption, International journal of hydrogen energy 45 (29) (2020) 14625–14639.

[22] A. Abdol Rahim, A. S. Tijani, S. Kamarudin, S. Hanapi, An overview of polymer electrolyte membrane electrolyzer for hydrogen production: Modeling and mass transport, Journal of Power Sources 309 (2016) 56–65.

[23] D. Falcão, A. Pinto, A review on pem electrolyzer modelling: Guidelines for beginners, Journal of cleaner production 261 (2020) 121184.

[24] P. Olivier, C. Bourasseau, P. B. Bouamama, Low-temperature electrolysis system modelling: A review, Renewable and Sustainable Energy Reviews 78 (2017) 280–300.

[25] L. Järvinen, P. Puranen, A. Kosonen, V. Ruuskanen, J. Ahola, P. Kauranen, M. Hehemann, Automized parametrization of pem and alkaline water electrolyzer polarisation curves, International Journal of Hydrogen Energy (2022).

[26] M. Maier, K. Smith, J. Dodwell, G. Hinds, P. Shearing, D. Brett, Mass transport in pem water electrolysers: A review, International Journal of Hydrogen Energy 47 (1) (2022) 30–56.

[27] V. Das, S. Padmanaban, K. Venkitusamy, R. Selvamuthukumaran, F. Blaabjerg, P. Siano, Recent advances and challenges of fuel cell based power system architectures and control–a review, Renewable and Sustainable Energy Reviews 73 (2017) 10–18.

[28] W. Daud, R. Rosli, E. Majlan, S. Hamid, R. Mohamed, T. Husaini, Pem fuel cell system control: A review, Renewable Energy 113 (2017) 620–638.

[29] B. Yang, J. Li, Y. Li, Z. Guo, K. Zeng, H. Shu, P. Cao, Y. Ren, A critical survey of proton exchange membrane fuel cell system control: Summaries, advances, and perspectives, International Journal of Hydrogen Energy (2022).

[30] C. Haas, M.-G. Macherhammer, N. Klopcic, A. Trattner, Capabilities and limitations of 3d-cfd simulation of anode flow fields of high-pressure pem water electrolysis, Processes 9 (6) (2021) 968.

[31] M. Carmo, D. L. Fritz, J. Mergel, D. Stolten, A comprehensive review on pem water electrolysis, International journal of hydrogen energy 38 (12) (2013) 4901–4934.

[32] D. M. Bernardi, M. W. Verbrugge, Mathematical model of a gas diffusion electrode bonded to a polymer electrolyte, AIChE journal 37 (8) (1991) 1151–1163.

[33] J. Baschuk, X. Li, A general formulation for a mathematical pem fuel cell model, Journal of power sources 142 (1-2) (2005) 134–153.

[34] S. Pasricha, S. R. Shaw, A dynamic pem fuel cell model, IEEE Transactions on Energy Conversion 21 (2) (2006) 484–490.

[35] Z. Abdin, C. Webb, E. M. Gray, Modelling and simulation of a proton exchange membrane (pem) electrolyser cell, International Journal of Hydrogen Energy 40 (39) (2015) 13243–13257.

[36] A. M. Abomazid, N. A. El-Taweel, H. E. Farag, Novel analytical approach for parameters identification of pem electrolyzer, IEEE Transactions on Industrial Informatics 18 (9) (2021) 5870–5881.

[37] E. Afshari, S. Khodabakhsh, N. Jahantigh, S. Toghyani, Performance assessment of gas crossover phenomenon and water transport mechanism in high pressure pem electrolyzer, International Journal of Hydrogen Energy 46 (19) (2021) 11029–11040.

[38] K. Agbli, M. Péra, D. Hissel, O. Rallières, C. Turpin, I. Doumbia, Multiphysics simulation of a pem electrolyser: Energetic macroscopic representation approach, International journal of hydrogen energy 36 (2) (2011) 1382–1398.

[39] P. Ahmadi, I. Dincer, M. A. Rosen, Energy and exergy analyses of hydrogen production via solar-boosted ocean thermal energy conversion and pem electrolysis, International Journal of Hydrogen Energy 38 (4) (2013) 1795–1805.

[40] F. Aubras, J. Deseure, J.-J. Kadjo, I. Dedigama, J. Majasan, B. Grondin-

Perez, J.-P. Chabriat, D. Brett, Two-dimensional model of low-pressure pem electrolyser: Two-phase flow regime, electrochemical modelling and experimental validation, International journal of hydrogen energy 42 (42) (2017) 26203–26216.
[41] A. Awasthi, K. Scott, S. Basu, Dynamic modeling and simulation of a proton exchange membrane electrolyzer for hydrogen production, International journal of hydrogen energy 36 (22) (2011) 14779–14786.
[42] C. Biaku, N. Dale, M. Mann, H. Salehfar, A. Peters, T. Han, A semiempirical study of the temperature dependence of the anode charge transfer coefficient of a 6 kw pem electrolyzer, International journal of hydrogen energy 33 (16) (2008) 4247–4254.
[43] M. Chandesris, V. Médeau, N. Guillet, S. Chelghoum, D. Thoby, F. Fouda-Onana, Membrane degradation in pem water electrolyzer: Numerical modeling and experimental evidence of the influence of temperature and current density, International Journal of Hydrogen Energy 40 (3) (2015) 1353–1366.
[44] P. Choi, D. G. Bessarabov, R. Datta, A simple model for solid polymer electrolyte (spe) water electrolysis, Solid State Ionics 175 (1-4) (2004) 535–539.
[45] F. da Costa Lopes, E. H. Watanabe, Experimental and theoretical development of a pem electrolyzer model applied to energy storage systems, in: 2009 Brazilian power electronics conference, IEEE, 2009, pp. 775–782.
[46] N. Dale, M. Mann, H. Salehfar, Semiempirical model based on thermodynamic principles for determining 6 kw proton exchange membrane electrolyzer stack characteristics, Journal of Power Sources 185 (2) (2008) 1348–1353.
[47] M. Espinosa-López, C. Darras, P. Poggi, R. Glises, P. Baucour, A. Rakotondrainibe, S. Besse, P. Serre-Combe, Modelling and experimental validation of a 46 kw pem high pressure water electrolyzer, Renewable energy 119 (2018) 160–173.
[48] P. Fragiacomo, M. Genovese, Modeling and energy demand analysis of a scalable green hydrogen production system, International Journal of Hydrogen Energy 44 (57) (2019) 30237–30255.
[49] P. Gabrielli, B. Flamm, A. Eichler, M. Gazzani, J. Lygeros, M. Mazzotti, Modeling for optimal operation of pem fuel cells and electrolyzers, in: 2016 IEEE 16th international conference on environment and electrical engineering (EEEIC), IEEE, 2016, pp. 1–7.
[50] R. García-Valverde, N. Espinosa, A. Urbina, Simple pem water electrolyser model and experimental validation, international journal of hydrogen energy 37 (2) (2012) 1927–1938.
[51] H. Görgün, Dynamic modelling of a proton exchange membrane (pem) electrolyzer, International journal of hydrogen energy 31 (1) (2006) 29–38.
[52] S. Grigoriev, A. Kalinnikov, P. Millet, V. Porembsky, V. Fateev, Mathematical modeling of high-pressure pem water electrolysis, Journal of applied electrochemistry 40 (2010) 921–932.
[53] B. Han, S. M. Steen III, J. Mo, F.-Y. Zhang, Electrochemical performance modeling of a proton exchange membrane electrolyzer cell for hydrogen energy, International Journal of Hydrogen Energy 40 (22) (2015) 7006–7016.
[54] R. Keller, E. Rauls, M. Hehemann, M. Müller, M. Carmo, An adaptive model-based feedforward temperature control of a 100 kw pem electrolyzer, Control Engineering Practice 120 (2022) 104992.
[55] H. Kim, M. Park, K. S. Lee, One-dimensional dynamic modeling of a high-pressure water electrolysis system for hydrogen production, International Journal of Hydrogen Energy 38 (6) (2013) 2596–2609.
[56] M. Koundi, H. EL FADIL, Mathematical modeling of pem electrolyzer and design of a voltage controller by the smpwm approach, in: 2019 International Conference on Power Generation Systems and Renewable Energy Technologies (PGSRET), IEEE, 2019, pp. 1–6.
[57] M. Lebbal, S. Lecœuche, Identification and monitoring of a pem electrolyser based on dynamical modelling, International journal of hydrogen energy 34 (14) (2009) 5992–5999.
[58] B. Lee, K. Park, H.-M. Kim, Dynamic simulation of pem water electrolysis and comparison with experiments, International journal of electrochemical science 8 (1) (2013) 235–248.
[59] V. Liso, G. Savoia, S. S. Araya, G. Cinti, S. K. Kær, Modelling and experimental analysis of a polymer electrolyte membrane water electrolysis cell at different operating temperatures, Energies 11 (12) (2018) 3273.
[60] F. Marangio, M. Santarelli, M. Calì, Theoretical model and experimental analysis of a high pressure pem water electrolyser for hydrogen production, International journal of hydrogen energy 34 (3) (2009) 1143–1158.
[61] B. Mohamed, B. Alli, B. Ahmed, Using the hydrogen for sustainable energy storage: Designs, modeling, identification and simulation membrane behavior in pem system electrolyser, Journal of Energy Storage 7 (2016) 270–285.
[62] F. Moradi Nafchi, E. Afshari, E. Baniasadi, N. Javani, A parametric study of polymer membrane electrolyser performance, energy and exergy analyses, International Journal of Hydrogen Energy 44 (34) (2019) 18662–18670.
[63] M. Ni, M. K. Leung, D. Y. Leung, Energy and exergy analysis of hydrogen production by a proton exchange membrane (pem) electrolyzer plant, Energy conversion and management 49 (10) (2008) 2748–2756.
[64] G. S. Ogumerem, E. N. Pistikopoulos, Dynamic modeling and explicit control of a pem water electrolysis process, Smart and Sustainable Manufacturing Systems 2 (2018) 25–43.
[65] E. T. Ojong, J. T. H. Kwan, A. Nouri-Khorasani, A. Bonakdarpour, D. P. Wilkinson, T. Smolinka, Development of an experimentally validated semi-empirical fully-coupled performance model of a pem electrolysis cell with a 3-d structured porous transport layer, International journal of hydrogen energy 42 (41) (2017) 25831–25847.
[66] P. Olivier, C. Bourasseau, B. Bouamama, Dynamic and multiphysic pem electrolysis system modelling: A bond graph approach, International Journal of Hydrogen Energy 42 (22) (2017) 14872–14904.
[67] A. A. Rahim, A. S. Tijani, F. H. Shukri, S. Hanapi, K. Sainan, Mathematical modelling and simulation analysis of pem electrolyzer system for hydrogen production (2014).
[68] V. Ruuskanen, J. Koponen, K. Huoman, A. Kosonen, M. Niemelä, J. Ahola, Pem water electrolyzer model for a power-hardware-in-loop simulator, International Journal of Hydrogen Energy 42 (16) (2017) 10775–10784.
[69] R. Sarrias-Mena, L. M. Fernández-Ramírez, C. A. García-Vázquez, F. Jurado, Electrolyzer models for hydrogen production from wind energy systems, International Journal of Hydrogen Energy 40 (7) (2015) 2927–2938.
[70] M. Sartory, E. Wallnöfer-Ogris, P. Salman, T. Fellinger, M. Justl, A. Trattner, M. Klell, Theoretical and experimental analysis of an asymmetric high pressure pem water electrolyser up to 155 bar, International Journal of Hydrogen Energy 42 (52) (2017) 30493–30508.
[71] S. Sawada, T. Yamaki, T. Maeno, M. Asano, A. Suzuki, T. Terai, Y. Maekawa, Solid polymer electrolyte water electrolysis systems for hydrogen production based on our newly developed membranes, part i: analysis of voltage–current characteristics, Progress in Nuclear Energy 50 (2-6) (2008) 443–448.
[72] M. Schalenbach, M. Carmo, D. L. Fritz, J. Mergel, D. Stolten, Pressurized pem water electrolysis: Efficiency and gas crossover, International Journal of Hydrogen Energy 38 (35) (2013) 14921–14933.
[73] F. Scheepers, M. Stähler, A. Stähler, E. Rauls, M. Müller, M. Carmo, W. Lehnert, Improving the efficiency of pem electrolyzers through membrane-specific pressure optimization, Energies 13 (3) (2020) 612.
[74] F. Scheepers, M. Stähler, A. Stähler, E. Rauls, M. Müller, M. Carmo, W. Lehnert, Temperature optimization for improving polymer electrolyte membrane-water electrolysis system efficiency, Applied Energy 283 (2021) 116270.
[75] C. Schnuelle, T. Wassermann, D. Fuhrlaender, E. Zondervan, Dynamic hydrogen production from pv & wind direct electricity supply–modeling and techno-economic assessment, International Journal of Hydrogen Energy 45 (55) (2020) 29938–29952.
[76] S. Sood, O. Prakash, M. Boukerdja, J.-Y. Dieulot, B. Ould-Bouamama, M. Bressel, A.-L. Gehin, Generic dynamical model of pem electrolyser under intermittent sources, Energies 13 (24) (2020) 6556.
[77] A. Tabanjat, M. Becherif, M. Emziane, D. Hissel, H. Ramadan, B. Mahmah, Fuzzy logic-based water heating control methodology for the efficiency enhancement of hybrid pv–pem electrolyser systems, international journal of hydrogen energy 40 (5) (2015) 2149–2161.
[78] A. S. Tijani, A. A. Rahim, Numerical modeling the effect of operating variables on faraday efficiency in pem electrolyzer, Procedia Technology 26 (2016) 419–427.
[79] A. S. Tijani, M. A. Ghani, A. A. Rahim, I. K. Muritala, F. A. B. Mazlan, Electrochemical characteristics of (pem) electrolyzer under influ-

ence of charge transfer coefficient, international journal of hydrogen energy 44 (50) (2019) 27177–27189.
[80] G. Tjarks, A. Gibelhaus, F. Lanzerath, M. Müller, A. Bardow, D. Stolten, Energetically-optimal pem electrolyzer pressure in power-to-gas plants, Applied energy 218 (2018) 192–198.
[81] S. Toghyani, S. Fakhradini, E. Afshari, E. Baniasadi, M. Y. A. Jamalabadi, M. S. Shadloo, Optimization of operating parameters of a polymer exchange membrane electrolyzer, International Journal of Hydrogen Energy 44 (13) (2019) 6403–6414.
[82] T. Yigit, O. F. Selamet, Mathematical modeling and dynamic simulink simulation of high-pressure pem electrolyzer system, International Journal of Hydrogen Energy 41 (32) (2016) 13901–13914.
[83] H. Zhang, S. Su, G. Lin, J. Chen, Efficiency calculation and configuration design of a pem electrolyzer system for hydrogen production, International journal of electrochemical science 7 (4) (2012) 4143–4157.
[84] D. Zhao, Q. He, J. Yu, J. Jiang, X. Li, M. Ni, Dynamic behaviour and control strategy of high temperature proton exchange membrane electrolyzer cells (ht-pemecs) for hydrogen production, International Journal of Hydrogen Energy 45 (51) (2020) 26613–26622.
[85] D. Zhao, Q. He, J. Yu, M. Guo, J. Fu, X. Li, M. Ni, A data-driven digital-twin model and control of high temperature proton exchange membrane electrolyzer cells, International Journal of Hydrogen Energy (2022).
[86] S. Grigoriev, V. Porembskiy, S. Korobtsev, V. Fateev, F. Auprêtre, P. Millet, High-pressure pem water electrolysis and corresponding safety issues, International journal of hydrogen energy 36 (3) (2011) 2721–2728.
[87] H.-S. Shin, B. S. Oh, Water transport according to temperature and current in pem water electrolyzer, International Journal of Hydrogen Energy 45 (1) (2020) 56–63.
[88] P. Trinke, B. Bensmann, R. Hanke-Rauschenbach, Current density effect on hydrogen permeation in pem water electrolyzers, International Journal of Hydrogen Energy 42 (21) (2017) 14355–14366.
[89] P. Trinke, G. Keeley, M. Carmo, B. Bensmann, R. Hanke-Rauschenbach, Elucidating the effect of mass transport resistances on hydrogen crossover and cell performance in pem water electrolyzers by varying the cathode ionomer content, Journal of The Electrochemical Society 166 (8) (2019) F465.
[90] O. Atlam, M. Kolhe, Equivalent electrical model for a proton exchange membrane (pem) electrolyser, Energy Conversion and management 52 (8-9) (2011) 2952–2957.
[91] A. Beainy, N. Karami, N. Moubayed, Simulink model for a pem electrolyzer based on an equivalent electrical circuit, in: International Conference on Renewable Energies for Developing Countries 2014, Ieee, 2014, pp. 145–149.
[92] D. Guilbert, G. Vitale, Dynamic emulation of a pem electrolyzer by time constant based exponential model, Energies 12 (4) (2019) 750.
[93] D. Guilbert, B. Yodwong, W. Kaewmanee, M. Phattanasak, M. Hinaje, Hydrogen flow rate control of a proton exchange membrane electrolyzer, in: 2019 Research, Invention, and Innovation Congress (RI2C), IEEE, 2019, pp. 1–6.
[94] D. Guilbert, G. Vitale, Improved hydrogen-production-based power management control of a wind turbine conversion system coupled with multistack proton exchange membrane electrolyzers, Energies 13 (5) (2020) 1239.
[95] Á. Hernández-Gómez, V. Ramirez, D. Guilbert, B. Saldivar, Development of an adaptive static-dynamic electrical model based on input electrical energy for pem water electrolysis, International Journal of Hydrogen Energy 45 (38) (2020) 18817–18830.
[96] Á. Hernández-Gómez, V. Ramirez, D. Guilbert, B. Saldivar, Cell voltage static-dynamic modeling of a pem electrolyzer based on adaptive parameters: Development and experimental validation, Renewable Energy 163 (2021) 1508–1522.
[97] Q. Feng, G. Liu, B. Wei, Z. Zhang, H. Li, H. Wang, et al., A review of proton exchange membrane water electrolysis on degradation mechanisms and mitigation strategies, Journal of Power Sources 366 (2017) 33–55.
[98] A. Weiss, A. Siebel, M. Bernt, T. H. Shen, V. Tileli, H. A. Gasteiger, Impact of intermittent operation on lifetime and performance of a pem water electrolyzer (Apr 2019).
[99] S. Sun, Z. Shao, H. Yu, G. Li, B. Yi, Investigations on degradation of the long-term proton exchange membrane water electrolysis stack (Jun 2014).
[100] A. C. Bhosale, S. Meenakshi, P. C. Ghosh, Root cause analysis of the degradation in a unitized regenerative fuel cell (Jan 2017).
[101] M. S. Thomassen, A. H. Reksten, A. O. Barnett, T. Khoza, K. Ayers, Pem water electrolysis (Oct 2021).
[102] G. Papakonstantinou, G. Algara-Siller, D. Teschner, T. Vidaković-Koch, R. Schlögl, K. Sundmacher, Degradation study of a proton exchange membrane water electrolyzer under dynamic operation conditions, Applied Energy 280 (2020).
[103] M. W. Fowler, R. F. Mann, J. C. Amphlett, B. A. Peppley, P. R. Roberge, Incorporation of voltage degradation into a generalised steady state electrochemical model for a pem fuel cell, Journal of power sources 106 (1-2) (2002) 274–283.
[104] W. Bi, T. F. Fuller, Modeling of pem fuel cell pt/c catalyst degradation, Journal of Power Sources 178 (1) (2008) 188–196.
[105] L. Placca, R. Kouta, Fault tree analysis for pem fuel cell degradation process modelling, International Journal of Hydrogen Energy 36 (2011).
[106] B. Yodwong, D. Guilbert, M. Phattanasak, W. Kaewmanee, M. Hinaje, G. Vitale, Faraday's efficiency modeling of a proton exchange membrane electrolyzer based on experimental data, Energies 13 (18) (2020) 4792.
[107] F. Khatib, T. Wilberforce, O. Ijaodola, E. Ogungbemi, Z. El-Hassan, A. Durrant, J. Thompson, A. Olabi, Material degradation of components in polymer electrolyte membrane (pem) electrolytic cell and mitigation mechanisms: A review, Renewable and Sustainable Energy Reviews 111 (2019) 1–14.
[108] M. Bernt, J. Schröter, M. Möckl, H. Gasteiger, Analysis of gas permeation phenomena in a pem water electrolyzer operated at high pressure and high current density, Journal of The Electrochemical Society 167 (12) (2020) 124502.
[109] T. Nagpure, Z. Chen, Control-oriented modeling of ionic polymer-metal composite enabled hydrogen gas production, International Journal of Hydrogen Energy 41 (16) (2016) 6619–6629.
[110] A. L. J. Keow, Z. Chen, Auto-tuning control of proton exchange membrane water electrolyzer with self-assessment and gain scheduling, Journal of Dynamic Systems, Measurement, and Control 143 (5) (2021).
[111] N. Chiesa, M. Korpås, O. Kongstein, A. Ødegård, Dynamic control of an electrolyser for voltage quality enhancement, in: proc of, 2011.
[112] A. Garrigós, J. Lizán, J. Blanes, R. Gutiérrez, Combined maximum power point tracking and output current control for a photovoltaic-electrolyser dc/dc converter, International journal of hydrogen energy 39 (36) (2014) 20907–20919.
[113] M. Albarghot, L. Rolland, Matlab/simulink modelling and experimental results of a pem electrolyzer powered by a solar panel, in: 2016 IEEE Electrical Power and Energy Conference (EPEC), IEEE, 2016, pp. 1–6.
[114] J. Koponen, A. Kosonen, V. Ruuskanen, K. Huoman, M. Niemelä, J. Ahola, Control and energy efficiency of pem water electrolyzers in renewable energy systems, International journal of hydrogen energy 42 (50) (2017) 29648–29660.
[115] V. Guida, D. Guilbert, G. Vitale, B. Douine, Design and realization of a stacked interleaved dc–dc step-down converter for pem water electrolysis with improved current control, Fuel Cells 20 (3) (2020) 307–315.
[116] P. Lettenmeier, R. Wang, R. Abouatallah, S. Helmly, T. Morawietz, R. Hiesgen, S. Kolb, F. Burggraf, J. Kallo, A. S. Gago, et al., Durable membrane electrode assemblies for proton exchange membrane electrolyzer systems operating at high current densities, Electrochimica Acta 210 (2016) 502–511.
[117] V. Ruuskanen, J. Koponen, A. Kosonen, M. Niemelä, J. Ahola, A. Hämäläinen, Power quality and reactive power of water electrolyzers supplied with thyristor converters, Journal of Power Sources 459 (2020) 228075.
[118] S. H. Frensch, F. Fouda-Onana, G. Serre, D. Thoby, S. S. Araya, S. K. Kær, Influence of the operation mode on pem water electrolysis degradation, International Journal of Hydrogen Energy 44 (57) (2019) 29889–29898.
[119] M. Müller, M. Carmo, A. Glüsen, M. Hehemann, S. Saba, W. Zwaygardt, D. Stolten, Water management in membrane electrolysis and options for advanced plants, International journal of hydrogen energy 44 (21) (2019) 10147–10155.
[120] J. C. Garcia-Navarro, M. Schulze, K. A. Friedrich, Detecting and modeling oxygen bubble evolution and detachment in proton exchange membrane water electrolyzers, International Journal of Hydrogen Energy

44 (50) (2019) 27190–27203.
[121] C. Immerz, M. Schweins, P. Trinke, B. Bensmann, M. Paidar, T. Bystroň, K. Bouzek, R. Hanke-Rauschenbach, Experimental characterization of inhomogeneity in current density and temperature distribution along a single-channel pem water electrolysis cell, Electrochimica acta 260 (2018) 582–588.
[122] S. Dahbi, R. Aboutni, A. Aziz, N. Benazzi, M. Elhafyani, K. Kassmi, Optimised hydrogen production by a photovoltaic-electrolysis system dc/dc converter and water flow controller, International Journal of Hydrogen Energy 41 (45) (2016) 20858–20866.
[123] K. Meier, Hydrogen production with sea water electrolysis using norwegian offshore wind energy potentials, International Journal of Energy and Environmental Engineering 5 (2) (2014) 1–12.
[124] M. Khan, T. Al-Attas, S. Roy, M. M. Rahman, N. Ghaffour, V. Thangadurai, S. Larter, J. Hu, P. M. Ajayan, M. G. Kibria, Seawater electrolysis for hydrogen production: a solution looking for a problem?, EnergyEnvironmental Science 14 (9) (2021) 4831–4839.
[125] B. Bensmann, R. Hanke-Rauschenbach, I. P. Arias, K. Sundmacher, Energetic evaluation of high pressure pem electrolyzer systems for intermediate storage of renewable energies, Electrochimica Acta 110 (2013) 570–580.
[126] B. Bensmann, R. Hanke-Rauschenbach, G. Müller-Syring, M. Henel, K. Sundmacher, Optimal configuration and pressure levels of electrolyzer plants in context of power-to-gas applications, Applied energy 167 (2016) 107–124.
[127] B. Bensmann, R. Hanke-Rauschenbach, K. Sundmacher, In-situ measurement of hydrogen crossover in polymer electrolyte membrane water electrolysis, International journal of hydrogen energy 39 (1) (2014) 49–53.
[128] J. Kim, E. Muljadi, R. M. Nelms, Modelling and control coordination scheme of a wind-to-hydrogen set for future renewable-based power systems, IET Renewable Power Generation 14 (17) (2020) 3317–3326.
[129] B. Flamm, C. Peter, F. N. Büchi, J. Lygeros, Electrolyzer modeling and real-time control for optimized production of hydrogen gas, Applied Energy 281 (2021) 116031.
[130] M. H. Cano, S. Kelouwani, K. Agbossou, Y. Dubé, Power management system for off-grid hydrogen production based on uncertainty, International Journal of hydrogen energy 40 (23) (2015) 7260–7272.
[131] A. J. Calderón, I. González, M. Calderón, Management of a pem electrolyzer in hybrid renewable energy systems, in: Fuzzy Modeling and Control: Theory and Applications, Springer, 2014, pp. 217–234.
[132] K. Sankar, A. K. Jana, Nonlinear control of a pem fuel cell integrated system with water electrolyzer, Chemical Engineering Research and Design 171 (2021) 150–167.
[133] E. N. Pistikopoulos, N. A. Diangelakis, R. Oberdieck, M. M. Papathanasiou, I. Nascu, M. Sun, Paroc—an integrated framework and software platform for the optimisation and advanced model-based control of process systems, Chemical Engineering Science 136 (2015) 115–138.